

Review

A Review: Photocatalysts Based on BiOCl and g-C₃N₄ for Water Purification

Qiang Ren ¹, Juming Liu ², Qi Yang ^{1,*} and Wei Shen ^{3,*}

¹ School of Water Resources and Environment, China University of Geosciences (Beijing), Beijing 100084, China; mars103@126.com

² School of Chemical Engineering, Inner Mongolia University of Technology, Huhhot 010051, China; liujuming@imut.edu.cn

³ China Waterborne Transport Research Institute, Ministry of Transport of the People's Republic of China, Beijing 100088, China

* Correspondence: yq@cugb.edu.cn (Q.Y.); shenwei@wti.ac.cn (W.S.)

Abstract: Many organic pollutants are discharged into the environment, which results in the frequent detection of organic pollutants in surface water and underground water. Some of the organic pollutants can stay for a long time in the environment due to their recalcitrance. Advanced oxidation processes (AOPs) can effectively treat the recalcitrant organic compounds in water. Photocatalysis as one of the AOPs has attracted a lot of interest. BiOCl and g-C₃N₄ are nice photocatalysts. However, their catalytic activity should be further improved for industrial utilization. The construction of heterojunction between the two different components is deemed as an efficient strategy for developing a highly efficient photocatalyst. As a typical type-II heterojunction, g-C₃N₄/BiOCl heterojunctions showed better photocatalytic performance. To date, the g-C₃N₄/BiOCl composites were mainly studied in the field of water purification. The photoactivity of the pristine catalysts was greatly enhanced by the combination of the two materials. However, three kinds of proposed mechanisms were used to explain the improvement of the g-C₃N₄/BiOCl heterojunctions. But few researchers tried to explain why there were three different scenarios employed to explain the charge transfer. According to the articles reviewed, no direct evidence could indicate whether the band structures of the heterojunctions based on BiOCl and g-C₃N₄ were changed. Therefore, many more studies are needed to reveal the truth. Having a clearer understanding of the mechanism is beneficial for researchers to construct more efficient photocatalysts. This article is trying to start a new direction of research to inspire more researchers to prepare highly effective photocatalysts.



Citation: Ren, Q.; Liu, J.; Yang, Q.; Shen, W. A Review: Photocatalysts Based on BiOCl and g-C₃N₄ for Water Purification. *Catalysts* **2021**, *11*, 1084. <https://doi.org/10.3390/catal11091084>

Academic Editors: Ioan Balint and Monica Pavel

Received: 19 August 2021

Accepted: 6 September 2021

Published: 8 September 2021

Publisher's Note: MDPI stays neutral with regard to jurisdictional claims in published maps and institutional affiliations.



Copyright: © 2021 by the authors. Licensee MDPI, Basel, Switzerland. This article is an open access article distributed under the terms and conditions of the Creative Commons Attribution (CC BY) license (<https://creativecommons.org/licenses/by/4.0/>).

1. Introduction

With the development of human civilization, many refractory pollutants were discharged to the environment, which are hard to be degraded by traditional purification methods. For example, pollutants like tetracycline [1], bisphenol A [2], Astrazole Black [3], estriol [4], and tetraethylated rhodamine [5] can hardly be degraded by normal waste-water treatment plants. Generally, the degradation of recalcitrant organic pollutants relies on the consumption of energy, such as the Fenton process. Photocatalysis has drawn much attention because of the utilization of solar energy and friendliness to the environment.

In photocatalysis, the heterojunction of two different materials is deemed as an efficient strategy to develop diverse hybrid composites with multiple functionalities [6]. Photocatalysts normally possess some defects that restrict the utilization of the material, for example, ultrafast recombination of photo-induced charge carriers [7], low efficient utilization of sunlight, and wide bandgap [8]. Hybridization of two different catalysts would be an excellent way to improve the photoactivity. Lots of photocatalysts were synthesized

in order to enhance the photoactivity of the catalysts, such as MoS₂/g-C₃N₄ [9], CuInS₂/g-C₃N₄ [10], Ag₂O/g-C₃N₄ [11], Ag₂O/TiO₂ [12], AgI/CuBi₂O₄ [13], CuS/BiVO₄ [14], Ag₃PO₄/MoS₂ [15], g-C₃N₄/SiO₂ [16], ZnFe₂O₄/TiO₂ [17], LaFeO₃/SnS₂ [18], Bi₂O₃/g-C₃N₄ [19], and Ag₂O/Bi₅O₇I [20]. Recently, heterojunctions based on BiOCl and g-C₃N₄ drew much attention because of the abundance of the materials in the environment.

Graphitic carbon nitride is regarded as a nice photocatalyst because of its nontoxicity, stability in pH over a broad range (0–14), easy to prepare, and the narrow bandgap [21]. After being first synthesized in 1834 [22], carbon nitride has been used in many areas, such as virus inactivation [23], activation of benzene [24], H₂ revolution [25,26], fuel cells [27], CO₂ reduction [28], and organic pollutants degradation [29]. However, because of its high recombination rate of the photogenerated charge carriers and low BET surface area, the application of g-C₃N₄ is restricted. Recently, many studies focused on building heterojunctions to improve its photoactivity, such as the system of WO₃/g-C₃N₄ [30], ZnWO₄/g-C₃N₄ [31], and In₂S₃/g-C₃N₄ [32]. According to these studies, coupling graphitic carbon nitride with other kinds of semiconductors could construct better photocatalysts by reducing the recombination rate of the photogenerated charge carriers or increasing the surface area.

On the contrary, layered structure of BiOCl facilitates the photogenerated charge carriers' separation and endows it with a strong ability to degrade organic pollutants [33]. Morphology control was employed by many researchers to improve the pristine catalyst [34]. For example, according to E. Ramírez Meneses and co-workers [35], the addition of capping agents could affect the morphology of BiOCl. However, the as-prepared catalysts were unable to be excited by visible light. In order to expand the light absorption range of BiOCl, many researchers synthesized heterostructures like carbon dots/BiOCl [36], BiOCl/g-C₃N₄ [37], WO₃/BiOCl [38], Bi₂MoO₆-BiOCl [33], BiOCl/BiOBr [39], m-Bi₂O₄/BiOCl [40], BiOCl/BiVO₄ [41], Bi₂O₂CO₃/BiOCl [42], and BiOI/BiOCl [43].

Among them, the composition of BiOCl and g-C₃N₄ is considered as an excellent combination. The heterojunction could enhance the separation of the photo-induced charge carriers and enable the catalyst to respond to visible light [43,44]. Noble metal doping is also considered as a good method to improve the semiconductor. However, the high cost of noble metal doping restricts its utilization. If a noble metal doping catalyst is used repeatedly, the catalyst will be eroded, and perhaps generate new pollutants [45]. Heterojunctions of semiconductors is friendly to the environment, stable, and abundant in nature. Especially, the system of g-C₃N₄/BiOCl could be used repeatedly and facile to be produced.

Some researchers also found the photoactivity of g-C₃N₄/BiOCl heterojunctions could be further enhanced by combining them with other materials. For example, the systems of Bi₂S₃/BiOCl/g-C₃N₄ [46], BiOCl/g-C₃N₄/kaolinite [47], and g-C₃N₄/CDs (carbon dots)/BiOCl [48]. Notably, through the addition of mediators, Z-scheme catalysts can be synthesized, such as the systems of g-C₃N₄/Au/BiOCl [49] and BiOCl/RGO/protonated g-C₃N₄ [50]. However, few researchers have focused on figuring out which method could prompt the photoactivity of the binary heterojunction. According to all the articles reviewed here, analysis of the proposed mechanism was an important section. Based on the adopted characterizations and experiments, the mechanism was discussed to help readers to understand the whole photocatalysis process.

First, in this article, the methods of preparation and the applications of the g-C₃N₄/BiOCl heterojunctions are reviewed. Then, the binary heterojunctions mentioned in this article were classified into three types according to the proposed mechanisms. The major difference between them is whether the alignment of band structures was taken into account after the syntheses. Many researchers carried out some experiments to prove their mechanisms. For instance, ESR and trapping experiments could demonstrate the main reactive species during the reaction. DFT (density functional theory) calculation was also adopted to anticipate the band structures and main reactive species [51]. However, all the methods seemed still not enough to directly prove the mechanism. Some of the studies seem controversial to each other. All three types of proposed mechanisms will be discussed in this article while

trying to find some patterns. Though dye sensitization happened when the heterojunctions were used to degrade some pollutant, this article tries to discuss whether the alignment of the band structure should be taken into account. At last, in the section of summary and outlook, the direction of the study on the mechanism is proposed.

2. Synthesis of g-C₃N₄/BiOCl Heterojunction

In the field of photocatalysis, g-C₃N₄ has been the focus of research in the past decade. Because the photo-induced electrons of g-C₃N₄ recombines with the hole very quickly. Though visible light accounts for more than 40% of solar light, this feature limits its utilization as a perfect photocatalyst.

The indirect band structure of BiOCl means photo-induced electron-hole pairs cannot recombine very quickly [8]. Furthermore, its layered structure facilitates the generation of the reactive species. The biggest problem is that this material only responds to UV-light, which merely accounts for 5% of solar light. This means BiOCl cannot make use of solar energy sufficiently.

In order to overcome the shortcomings of the semiconductors mentioned above, metal and carbonaceous materials were introduced [52]. Doping of those materials could improve charge separation and light absorption of the pristine catalysts. For example, noble metal with high electric conductivity and different Fermi level energy were doped into the semiconductor. The metal particles acted as the electron reservoirs or acceptors on the surface of the catalyst. However, holes generated on the semiconductor cannot migrate to noble metal particles because of the existence of the Schottky barrier. Thus, charge separation is realized through elemental doping [22]. However, doping of other materials has its limitations as mentioned above. None-metallic heterojunctions are becoming more attractive. The semiconductor-semiconductor hybridization is generally supposed to be an effective way to improve the photoactivity of the semiconductors. Composite of BiOCl and g-C₃N₄ is proved to be an excellent form of a heterojunction photocatalyst.

As it is known to us all, efficient methods to enhance the activity of photocatalyst can be divided into two types: (1) facilitating photo-induced charge separation; (2) improving the efficiency of solar energy utilization. There is no doubt that making a heterojunction between two different semiconductors is an excellent way to realize the two aims at the same time. Compositing BiOCl and g-C₃N₄ can not only improve charge carriers' separation, but also make the composite respond to visible light.

Heterojunctions of g-C₃N₄/BiOCl could be synthesized by many methods. According to the articles reviewed, there are three different methods overall employed by researchers, hydrothermal, deposition-precipitation, and solvent thermal. It is hard to say which one of them is the best. Generally, catalysts with larger surface area and thinner morphology could facilitate the degradation of pollutants. All the heterojunctions reviewed showed enhanced visible light absorption. Thus, it is reasonable to say the photoactivity of the catalysts was improved through the construction of the heterojunction.

Graphitic carbon nitride synthesized through calcination of urea showed higher surface area and better photoactivity [22]. Considering the theoretical specific surface area of perfect monolayer g-C₃N₄ is 2500 m² g⁻¹, there is still a long distance to cover [53]. However, it is not the main reason that explains the photocatalytic improvement of the composite based on the system of g-C₃N₄/BiOCl. The BET surface area of pristine g-C₃N₄ could be 150.10 m² g⁻¹, but the photoactivity is much lower than the hybrid. The surface area of BiOCl-CN_s-3% is much lower than BiOCl-CN_s-5%, whereas the photoactivity is much higher [6].

The mass ratio of the heterojunction is a very important factor. There is no doubt that the addition of BiOCl can prompt the photo-induced charge separation, and C₃N₄ can enhance the absorption of visible light in the systems. Theoretically, higher mass ratio of BiOCl means more chances for charge carriers to be separated, which could improve the photoactivity of the composite. When the mass ratio of one certain component increases, the photoactivity of the composite will not stop being enhanced until the generation of

and separation of photo-induced charge carriers reaches a certain balance. However, higher ratio of BiOCl does not always mean higher photoactivity. In the system of (20%) g-C₃N₄/BiOCl when the mass ratio of g-C₃N₄ reached 20%, the catalyst showed the best photocatalysis performance [21]. When the mass ratio was below 20%, increasing the ratio of g-C₃N₄ led to the photocatalytic enhancement of the heterojunction. If the mass ratio increased further, the activity started to decrease. Because too much g-C₃N₄ tends to agglomerate with itself, the contact between BiOCl and g-C₃N₄ was weakened [54]. The same thing happened when the mass ratio of BiOCl increased.

Generally, the morphology of g-C₃N₄ is hard to control unless using a certain template or different precursor [55]. Direct calcination of the precursors could only produce bulk g-C₃N₄. In order to improve the connection between the g-C₃N₄ and the BiOCl, exfoliation of the bulk g-C₃N₄ was adopted by many researchers. There are mainly three exfoliation methods that were adopted, chemical blowing, thermal, and liquid exfoliation. Previous researchers have proved that g-C₃N₄ exfoliated by thermal exfoliation method exhibited better photocatalytic performance than others through comparative experiments [56]. According to the articles reviewed, g-C₃N₄ commonly synthesized before the construction of the binary heterojunctions, so the construction of the heterojunction could not affect the morphology of g-C₃N₄. However, the presence of g-C₃N₄ could influence the morphology of BiOCl in the binary heterojunction. Therefore, the morphology control of BiOCl should be a very important factor that influences the photocatalytic performance of the binary heterojunction system under visible light irradiation.

Moreover, facet control of BiOCl is also a very efficient method to enhance photoactivity of the heterojunction. BiOCl with exposed 001 and 010 facets could be synthesized through PH value adjustment during the process of the construction route [57]. The better visible-light photocatalytic performance of BiOCl-010 could be attributed to the larger surface area, which could also benefit for the construction of the heterojunction.

2.1. Hydrothermal Method

Generally, in the hydrothermal method, g-C₃N₄ powder-prepared through polymerization was dispersed in deionized water, and then the solution was stirred in order to prepare a suspension. Commonly, Bi (NO₃)₃·5H₂O and KCl were added into the as-prepared suspension. Subsequently, the mixed suspension was transferred to an autoclave and heated to gain the BiOCl/g-C₃N₄. To date, three kinds of BiOCl/g-C₃N₄ heterojunction were prepared through the hydrothermal method (listed in Table 1).

Table 1. G-C₃N₄/BiOCl heterojunctions synthesized by hydrothermal method.

Catalyst (Mass Ratio %)	Template	Morphology	Size	Year	Ref.
BiOCl/g-C ₃ N ₄ (50/50)	SDBS	nanoplate	<5 nm	2017	[58]
g-C ₃ N ₄ /BiOCl (23.03/76.97)	-	nanodisc	35–50 nm	2017	[59]
BiOCl/g-C ₃ N ₄ (40/60)	-	-	2 μm	2015	[60]

Just as analyzed above, morphology of BiOCl is the most important variable in the process. Generally speaking, BiOCl of the BiOCl/g-C₃N₄ system with larger surface area is expected to show better visible light absorption. So, the main purpose of this section is to find out which method could make the morphology of BiOCl become thinner.

L. Song and co-workers employed NH₄Cl as blowing agent to make ultrathin g-C₃N₄ nanosheets (prepared by polymerization of melamine) in order to enhance the contact between the two materials [59]. In that article, two-dimensional g-C₃N₄/BiOCl heterojunctions were prepared through a facile hydrothermal method. The width of Pristine BiOCl is less than 3 μm and thicknesses is 50–60 nm. Notably, the construction of the binary heterojunction affected the morphology of the BiOCl. The thickness of nanodisc-like BiOCl was around 35–50 nm after loaded by ultrathin graphitic carbon nitride.

Yifan Yang and coworkers also adopted a hydrothermal method to synthesize the heterojunction [60]. Interestingly, before the construction of the g-C₃N₄/BiOCl heterojunction,

they synthesized g-C₃N₄ and BiOCl separately. After the formation of the heterojunction, it was observed that the width of BiOCl was 2 μm and the thickness was about 200 nm. Obviously, the surface area of the heterojunction should be smaller than that synthesized in the study mentioned above, though it showed better photoactivity than pristine catalysts.

According to Yongkui Huang and colleagues, they used BiCl₃ as a precursor to synthesize the heterojunction [58]. It was reported that nanoplate-shaped BiOCl decorated on the surface of g-C₃N₄ with thickness below 5 nm and widths of 20~30 nm. However, the result of X-ray powder diffraction (XRD) showed that the 001-facet exposed BiOCl and was the dominate, which is supposed to be beneficial for the UV-light photocatalytic reaction.

Especially, when it comes to visible-light, among all the articles reviewed in this section, though heterojunction synthesized by using BiCl₃ as precursor showed the thinnest structure, method employed by L. Song and co-workers should be the better way to synthesize g-C₃N₄/BiOCl heterojunction.

2.2. Deposition-Precipitation Method

Deposition-precipitation is another facile way to synthesize g-C₃N₄/BiOCl binary heterojunction. According to the studies reviewed, most researchers adopted this method to fabricate the heterojunction as listed in Table 2. Qingbo Li and co-workers proved that facet control was still the main factor that affected the photoactivity of the heterojunction under visible light illumination, though proper way of exfoliation could also improve the photocatalytic performance [61]. They synthesized g-C₃N₄, BiOCl-010, and BiOCl-001, separately, before the construction of the heterojunction. It was obvious that the BiOCl-010 possessed sharper edges and smaller size, according to Figure 1, which means its surface area was larger.

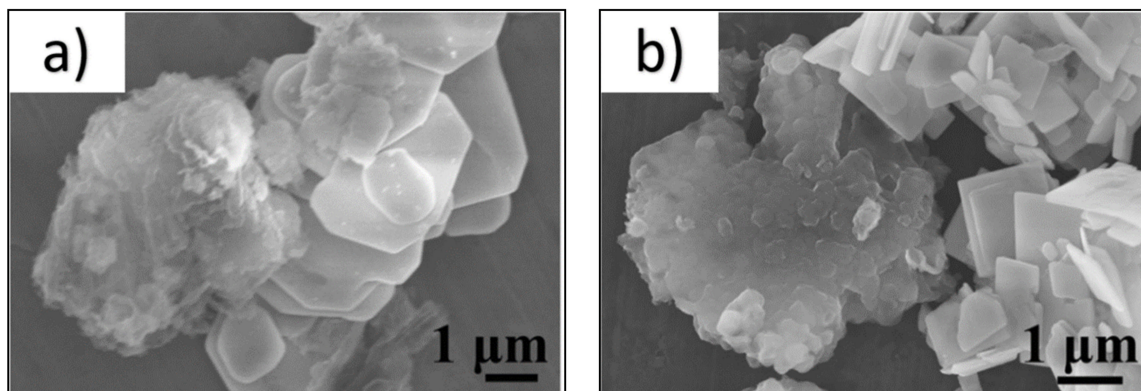


Figure 1. SEM images of (a) g-C₃N₄/BiOCl-001 and (b) g-C₃N₄/BiOCl-010. Reproduced with permission from Iqbal W et al, Catalysis Science & Technology; published by Royal Society of Chemistry, 2018.

Furthermore, the unique hierarchical flowerlike morphology of BiOCl could improve the photoactivity of the heterojunction because of its enlarged surface area [6]. This was proved by Liwen Lei and coworkers through synthesizing flower-like BiOCl by using Arabic gum (AG) as a template [34]. The heterojunction using AG showed better photocatalytic performance than that without using the template. Weidong Hou and coworkers also synthesized a flower-like g-C₃N₄/BiOCl heterojunction employing a microwave-assisted method [62]. However, the function of microwave was to accelerate the reaction process and to enhance the purity of the heterojunction [63,64]. Therefore, the utilization of microwave could not control the morphology of the composite. Compared to the study completed by Weidong Hou and colleagues, the presence of ethylene glycol could facilitate the formation of flower-like heterojunction. Tiekun Jia and colleagues also constructed a flower-like heterojunction by using ethylene glycol and glycerine [65]. The presence of glycerine increased the surface area of the composite.

Table 2. G-C₃N₄/BiOCl heterojunctions synthesized by deposition–precipitation method.

Catalyst (Mass Ratio %)	Template	Morphology	Size	BET Surface Area	Year	Ref.
BiOCl/g-C ₃ N ₄ (97/3)	-	Hierarchical flowerlike	0.15 μm/10 nm	19.04	2014	[6]
g-C ₃ N ₄ /BiOCl (20/80)	-	Nanoplate	1 μm	-	2014	[21]
C ₃ N ₄ /BiOCl (20/80)	Arabic gum	Flower-like	200 nm/5–8 nm	49.37	2014	[34]
ng-CN/BOC-010 (70/30)	-	Nanoparticle-nanosheet	-	18.10	2015	[61]
(OV)BiOCl/g-C ₃ N ₄ -10	-	Flower-like	2 μm/33.7 nm	11.66	2020	[62]
BiOCl/g-C ₃ N ₄ (10/90)	-	Sheet-like+ microplate	51.8 nm	-	2019	[63]
g-C ₃ N ₄ /BiOCl (55/45)	-	Hierarchical flower-like	1 μm/10 nm	44.2	2017	[65]
BiOCl-g-C ₃ N ₄	-	Two-dimensional structure	10 nm	-	2014	[66]
BiOCl-g-C ₃ N ₄ (50/50)	CTAC	Wrinkle two-dimensional structure	10 nm	-	2014	[67]
g-C ₃ N ₄ /BiOCl (20/80)	-	Nanoplate + sheets	1 μm	-	2015	[68]
BiOCl/(0.1g)g-C ₃ N ₄	-	nanosheet	20 nm	6.60	2017	[69]

Though it was observed that the presence of g-C₃N₄ during the synthesis of the BiOCl would make the morphology of BiOCl become thinner, the addition of some template could construct even thinner morphology, which means enlarged surface area. Yang Bai and coworkers synthesized a g-C₃N₄/BiOCl heterojunction by using cetyltrimethylammonium chloride (CTAC) as the template [66]. The size of the composite was about 10 nm. The template facilitated the formation of BiOCl nano-dots deposited on the surface of g-C₃N₄ as reported by Chun-zhi Zheng and colleagues [67]. However, if the heterojunction was synthesized without using any template, the morphology of the composite was supposed to be larger. Jiangbo Sun and coworkers constructed a g-C₃N₄/BiOCl-010 heterojunction just by adjusting the PH value [68]. The size of it was about 5 μm.

According to Lingjun Song and colleagues, the thickness of BiOCl decreased from 40 to 20 nm after combined with g-C₃N₄ [69]. The same phenomenon was observed by Weidong Hou and coworkers, the as-prepared flower-like BiOCl became thinner as the content of g-C₃N₄ increased [62]. The width and thickness of pristine BiOCl became smaller than 2 μm and 33.7 nm after the construction of the binary heterojunction, as demonstrated in Figure 2. Notably, among all the articles reviewed in this section, Shan Shi and colleagues employed NaBiO₃ to synthesize the g-C₃N₄/BiOCl heterojunction instead of Bi(NO₃)₃·5H₂O [21]. According to the study, though its size was about 1 μm, the BiOCl in the as-prepared heterojunction was 001 facets exposed, which could facilitate response to the UV light illumination. When it came to visible light photocatalytic reaction, the facile route adopted by Liwen Lei and coworkers could synthesize the heterojunction with larger surface area among all the deposition–precipitation methods reviewed.

2.3. Solvent-Thermal Method

The solvent thermal method is similar to the aforementioned hydrothermal method. The main difference is the starting materials of solvent thermal method are dissolved in some organic solvent while those of hydrothermal method dissolved in deionized water. All the g-C₃N₄/BiOCl heterojunctions synthesized by solvent thermal method are listed in Table 3.

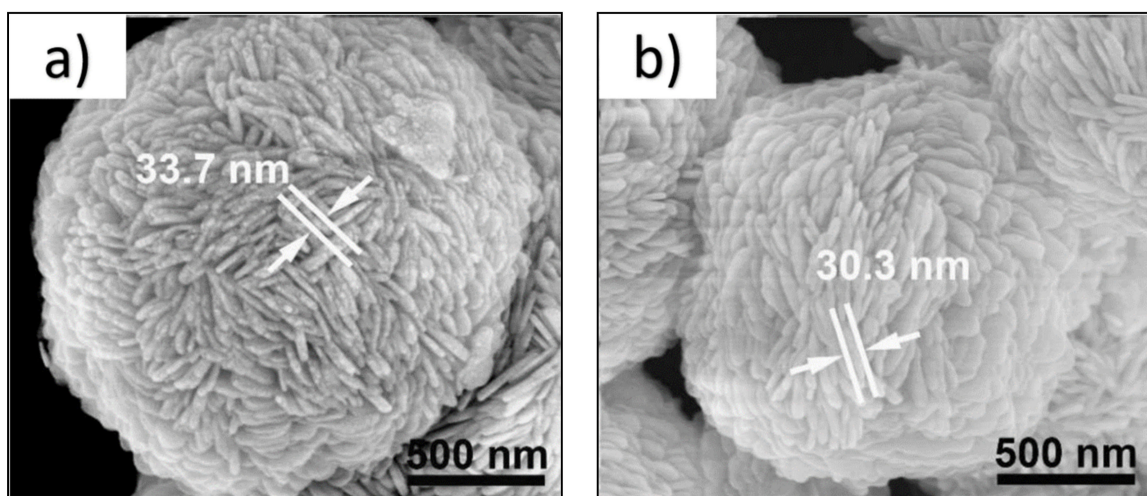


Figure 2. SEM images of (a) flower-like BiOCl and (b) g-C₃N₄/BiOCl. Reproduced with permission from Hou W et al., ChemistrySelect; published by John Wiley and Sons, 2020.

Table 3. G-C₃N₄/BiOCl heterojunctions synthesized by solvent thermal method.

Catalyst (Mass Ratio %)	Template	g-C ₃ N ₄ Precursor	Morphology	Diameter or Thickness	BET Surface Area (m ² /g)	Year	Ref.
BiOCl-C ₃ N ₄ (50/50)	IL: [HMIm]Cl	melamine	nanoflowers	-	24.26	2013	[44]
BiOCl/g-C ₃ N ₄ (85/15)	CTAB	melamine	rolled flake+ lamellar	70 nm	47.1	2019	[70]
(OV)BiOCl-g-C ₃ N ₄ (50/50)	PVP	urea	Ultrathin nanosheet	~4.3 nm	62.0	2017	[71]
BOC/CN (60/40)	-	melamine	ultrathin layered structure	around 3.5 nm	68.5	2019	[72]
BiOCl/C ₃ N ₄	-	urea	Nanoplate+ rough slice	-	47.1	2017	[73]
g-C ₃ N ₄ /BiOCl (1/99)	[C ₁₆ mim]Cl	Dicyandiamide'	three-dimensional spherical structure	1 μm	22.58	2016	[74]

Notably, the ionic liquid 1-hexyl-3-methylimidazolium chloride (IL: [HMIm]Cl) was used as one of the starting materials. It was used as a template and the source of chloride. For example, Xiao-jing Wang and colleagues prepared a novel g-C₃N₄/BiOCl heterojunction through a facile solvent thermal route [44]. According to the study, ionic liquid (IL: [HMIm]Cl) not only played an important role as the source of Cl, but also as a template to direct the growth of the nanoplate into flowerlike nanoparticles. The as-prepared g-C₃N₄/BiOCl composite was synthesized with larger surface area than the pristine catalysts and better photocatalytic performance. Ionic liquid was also adopted by other researchers, S. Yin and colleagues prepared a g-C₃N₄/BiOCl composite that employed the ionic liquid [C₁₆mim]Cl as the source of Cl [74]. Like the study mentioned above, Bi(NO₃)₃·5H₂O and ethylene glycol were used as starting materials. Similarly, the two composites showed a flower-like microsphere structure instead of the nano-slice structure. It is reasonable to believe that the presence of ionic liquid could direct the morphology of the g-C₃N₄/BiOCl heterojunction in these two studies. According to the XRD patterns of them, the BiOCl of the two heterojunctions were not 001 facet dominant like showed in Figure 3. This might mean the heterojunction could respond better to visible light than UV-light.

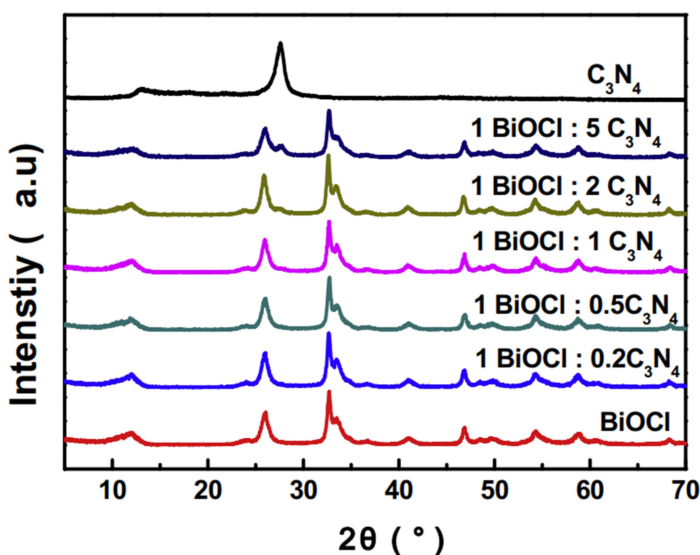


Figure 3. XRD patterns of BiOCl , C_3N_4 , and $\text{g-C}_3\text{N}_4/\text{BiOCl}$ heterojunction in different compositions. Reproduced with permission from Wang XJ et al, Chemical Engineering Journal; published by Elsevier BV, 2013.

Among all the heterojunctions synthesized through the solvent thermal method, only ionic liquid assisted routes could prepare flower-like $\text{g-C}_3\text{N}_4/\text{BiOCl}$ heterojunctions. There were other templates that researchers employed to regulate the morphology of the heterojunction. For instance, cetyltrimethyl ammonium bromide (CTAB) and urea were used by Wei Cai and colleagues to prepare a nano-sliced $\text{g-C}_3\text{N}_4/\text{BiOCl}$ heterojunction [70]. The construction of the heterojunction did not change the morphology of the BiOCl obviously. However, the presence of the template could not just direct the morphology. According to Qiao Wang and coworkers, the presence of the template could facilitate the generation of oxygen vacancies [71]. Unlike the aforementioned studies, NaCl was adopted as the source of Cl, and Polyvinylpyrrolidone (PVP) was used as the template. A facile solvent thermal method was adopted to prepare an ultrathin $\text{g-C}_3\text{N}_4/\text{BiOCl}$ heterojunction. Just like reported by Xianlong Zhang and colleagues [72], the formation of the heterojunction could make the morphology of the BiOCl become thinner. It was proved that the absence of PVP lowered the photoactivity of the heterojunction. Oxygen vacancies were supposed to act as the trap of electrons and facilitated the generation of superoxide radicals. The result of the density-functional calculation indicated that the presence of the oxygen vacancies narrowed the bandgap, thus improving the absorption of light.

Though the addition of some templates could help to prepare heterojunctions with thinner structure and enhance the photoactivity, the presence of them might cause some environmental problems. So, scientists adopted some template-free solvent thermal methods to prepare the binary heterojunction. Xianlong Zhang and colleagues synthesized a 2 D/2 D $\text{g-C}_3\text{N}_4/\text{BiOCl}$ composite via a solvent thermal method without the presence of any templates [72]. According to the study, HCl was used as the source of the Cl. The study indicated that ultrathin $\text{g-C}_3\text{N}_4/\text{BiOCl}$ nanosheets were prepared without the presence of any templates. The two pristine catalysts were self-assembled to form a face-to-face contact, which facilitated the charge transfer and the light absorption. Wenwen Liu and coworkers prepared a square-like nanoplates heterojunction without using templates [73]. NaCl aqueous solution was the source of the Cl. Compared to the study mentioned before, HCl might help to enlarge the surface area of the heterojunction.

Therefore, the heterojunction prepared through the template-free solvent thermal method adopted by Xianlong Zhang and colleagues showed the thinnest structure among all the solvent thermal methods. However, the as-prepared BiOCl was 001 facet dominant. It is reasonable to believe that the as-prepared catalyst would exhibit better photoactivity

under UV-light illumination. According to the articles reviewed, all the heterojunction were not 001 facet exposed, except that prepared by Xianlong Zhang and colleagues. So, when it comes to visible light illumination, heterojunction synthesized by Qiao Wang and coworkers could exhibit better photocatalytic performance than other catalysts because of its enlarged surface area.

2.4. Calcination Method

Besides the methods mentioned above, Wenjie Shan and colleagues synthesized the g-C₃N₄/BiOCl heterojunction through an in-situ calcination method [75]. They obtained a composite with enhanced photoactivity through the direct calcination of Bi₂O₃ and guanidine hydrochloride. Despite the different starting materials, the as-prepared composite showed superior catalytic performance and enlarged surface area ($25.50\text{ m}^2\text{ g}^{-1}$), similar to the flower-like structured g-C₃N₄/BiOCl heterojunctions synthesized through other methods. Notably, the 001 facet of as-prepared catalyst showed very strong signal. The heterojunction might show better photocatalytic performance under UV-light illumination.

Therefore, the methods employed to synthesize the g-C₃N₄/BiOCl binary photocatalyst mainly focused on making a thinner and hierarchical structure. Facilitating the charge transfer between the two components is one of the main purposes. The larger surface area might be beneficial for the enlarged interfacial contact area, which is why the thinner structured heterojunction exhibited obviously enhanced photoactivity compared to the pristine catalysts. It is believed larger surface area of one certain material could provide more active sites for the absorption of organic matters and photocatalytic reactions [45,76,77]. On one hand, higher surface area means higher mass to surface area rate and more area for other catalysts to deposit on it. On the other hand, enlarged surface area endows photocatalysts to absorb visible light more efficiently [41]. Among the articles reviewed, the exfoliation and introduction of organic template produced the thinner structured BiOCl heterojunction that possessed larger face-to-face interface with g-C₃N₄ and facilitated the efficient charge separation of light-induced charge carriers of the heterojunction system [65,71]. A similar pattern could be observed in other heterojunction systems [7,34,44,49,78]. However, whether a certain structure is beneficial for photoactivity generally depends on the circumstance [79]. The function of morphology still needs to be studied further to reveal a clearer pattern.

3. Applications of g-C₃N₄/BiOCl Heterojunction

To date, the g-C₃N₄/BiOCl heterojunction was mainly applied in the degradation of organic dyes, residual pharmaceutical agents, and plasticizers in aqueous solution. The heterojunction was not applied in fields of H₂ generation, CO₂ reduction, water splitting, or disinfection yet.

3.1. Dye Degradation

Organic dyes are widely used, particularly azo dyes, and are very difficult to be degraded by conventional biological treatment because of the complex aromatic structure, which is highly hazardous to the human race [80,81]. For example, RhB is almost unable to be degraded under irradiation of visible light without the addition of a photocatalyst [34]. Degradation of rhodamine B was employed repeatedly to test the photocatalytic performance of the g-C₃N₄/BiOCl composite. Methyl orange (MO) and methylene blue (MB) were also used to test photoactivity of the binary heterojunction. All the heterojunctions applied to dye degradation were listed in Table 4.

Table 4. G-C₃N₄/BiOCl heterojunctions applied to dye degradation.

Catalyst (Mass Ratio%)	Application	Efficiency/Time	Light Source	Concentration of the Pollutant	Main Reactive Species	Stability and Reusability	Ref.
BiOCl/g-C ₃ N ₄ (97/3)	Degradation of RhB	100%/40 min	400 W halogen lamp sodium nitrite solution (2 M) to eliminate UV light ($\lambda < 400$ nm) and thermal effect 500 W Xenon lamp with a light filter 400–800 nm	50 mg/L	•O ₂ [−]	stable after 7 irradiation cycles	[6]
g-C ₃ N ₄ /BiOCl (20/80) (001)	Degradation of RhB	100%/35 min	500 W Xe arc lamp UV-cut off filter ($\lambda > 420$ nm)	7 mg/L	-	65% after 10 irradiation cycles	[21]
C ₃ N ₄ /BiOCl (20/80)	Degradation of RhB	~100%/20 min	500 W Xe arc lamp UV-cut off filter ($\lambda > 420$ nm)	20 mg/L	•O ₂ [−] , hole	90% after 5 irradiation cycles	[34]
BiOCl-C ₃ N ₄ (50/50) (001)	Degradation methyl orange (MO)	95%/80 min	300 W xenon arc lamp 400 nm cutoff filter	10 mg/L	hole	stable after 6 irradiation cycles	[44]
BiOCl/g-C ₃ N ₄ (50/50) (001)	Degradation of RhB	>90%/50 min	300 W Xelamp 400 nm cutoff filter 300 W Xe arc lamp 400 nm cutoff filter 35 mW/cm ²	10 mg/L	-	-	[58]
g-C ₃ N ₄ /BiOCl (23.03/76.97)	Degradation of RhB	100%/30 min	500 W Xenon lamp 420 nm cutoff filter	10 mg/L	•O ₂ [−] , hole	stable after 4 irradiation cycles	[59]
BiOCl/g-C ₃ N ₄ (40/60) (001)	Degradation of methylene-blue (MB)	80%/120 min	500 W Xenon lamp 420 nm cutoff filter	5–10 mol/L	-	stable after 5 irradiation cycles	[60]
ng-CN/BOC-010 (70/30)	Degradation methyl orange (MO)	>90%/150 min	300 W metal-halide lamp 420 nm cutoff filter daylight lamp 60 W, $\lambda \geq 400$ nm	20 mg/L	•O ₂ [−] , hole	-	[61]
g-C ₃ N ₄ / BiOCl (55/45)	Degradation of methylene blue (MB)	100%/30 min	300 W xenon lamp incident lightpower: 6 W	5–10 mol/L	hole	~99% after 5 irradiation cycles	[65]
BiOCl-g-C ₃ N ₄	Degradation of RhB	99%/60 min	300 W xenon lamp	10 mg/L	•OH, •O ₂ [−]	-	[66]
BiOCl-g-C ₃ N ₄ (50/50)	Degradation of RhB	99%/35 min	500-W Xe lamp with a light filter 400–800 nm	10 mg/L	-	-	[67]
g-C ₃ N ₄ /BiOCl (20/80)	Degradation of RhB	100%/20 min	500-W Xe lamp with a light filter 400–800 nm	7 mg/L	-	56% after 5 irradiation cycles	[68]

Table 4. *Cont.*

Catalyst (Mass Ratio%)	Application	Efficiency/Time	Light Source	Concentration of the Pollutant	Main Reactive Species	Stability and Reusability	Ref.
BiOCl/(0.1 g)g-C ₃ N ₄ (001)	Degradation of RhB	100%/50 min	300 W Xe arc lamp 400 nm cutoff filter 35 mW/cm ²	10 mg/L	•O ₂ ⁻ , hole	stable after 5 irradiation cycles	[69]
BiOCl/g-C ₃ N ₄ (85/15)	Degradation of RhB	90%/30 min	300 W Xe lamp 400 nm cutoff filter	25 mg/L	•O ₂ ⁻	-	[70]
BOC/CN (60/40)	Degradation of RhB	95.93%/80 min	300 W Xe lamp 420 nm cutoff filter	10 mg/L	•O ₂ ⁻ , hole	89% after 5 irradiation cycles	[72]
BiOCl/C ₃ N ₄	Degradation of methyl orange (MO)	84.28%/180 min	0.5 mol·L ⁻¹ Na ₂ SO ₄ Solution ($\lambda \geq 420$ nm)	10 mg/L	•O ₂ ⁻ , hole	stable after 4 irradiation cycles	[73]
g-C ₃ N ₄ /BiOCl (1/99)	Degradation of RhB	94 %/30 min	300 W Xe lamp 400 nm cutoff filter	10 mg/L	•O ₂ ⁻ , hole	-	[74]
g-C ₃ N ₄ /BiOCl (001)	degradation of methyloorange (MO)	70%/300 min	500 W halogen tungsten lamp 420 nm cut-off filter	20 mg/L	-	stable after 4 irradiation cycles	[75]

The main defect that influences the photoactivity of g-C₃N₄ is the low separation efficiency of the photo-induced charge carriers. It is believed the layered structure of [Bi₂O₂]²⁺ blocks of bismuth oxyhalides (BiOX) could enhance the separation of the charge carriers [68]. This is why BiOX attracts the attentions of many researchers. Therefore, the introduction of BiOX could improve the photocatalytic performance of the binary heterojunction. Among heterojunctions of g-C₃N₄/BiOCl, g-C₃N₄/BiOBr, and g-C₃N₄/BiOI, g-C₃N₄/BiOCl composite showed the best visible light photocatalytic performance tested by degradation of RhB, according to J. Sun and colleagues [68]. So, the compositing of g-C₃N₄ and BiOCl could be a very efficient way to synthesize a better photocatalyst.

Obviously, the degradation rate of organic dyes was accelerated under visible-light illumination through the combination of the two pristine catalysts. Because of the dye sensitization, though RhB could be degraded over BiOCl under visible light irradiation, the introduction of g-C₃N₄ further enhanced the photocatalytic performance of the composite [67]. It was reported that the degradation efficiency could be about 25 times higher than pure g-C₃N₄ [6]. Y. Yang and colleagues introduced g-C₃N₄ into pristine BiOCl, then the degradation rate of MB was increased about 5.9 times higher under the illumination of visible light [60]. L. Song and coworkers demonstrated that the degradation rate of RhB reached 89 and 50% over pristine BiOCl and g-C₃N₄, respectively, while that of the as-prepared g-C₃N₄/BiOCl heterojunction reached almost 100% within 30 min of visible light irradiation [59].

As mentioned above, facet control could improve the photoactivity of the binary heterojunction greatly. The degradation rate of MO under visible light irradiation over ng-CN/BiOC-010 was about two times that over ng-CN/BiOC-001 [61,69]. Though prepared by different researchers, heterojunctions synthesized by 010 dominant BiOCl (010HB) showed improved photoactivity compared to 001 dominant BiOCl (001HB). According to the first ten heterojunctions listed in Table 4, though the concentration of RhB was different, 001HB could completely degrade RhB in about 50 min. Those prepared by 010HB showed better photoactivity. RhB could be degraded in about 30 min. The degradation rate of MB over 001HB was inferior to 010HB. 001HB could only remove MB in 2 h [60], while MB was degraded in 30 min over 010HB [65].

Just as discussed above, surface area is another crucial factor that influences the photoactivity of the heterojunction under visible light illumination. Yang Bai, Xianlong Zhang, and coworkers also synthesized 010HB [66,72], but the degradation of the model pollutant (RhB 10mg L⁻¹) lasted for about more than an hour. Whereas, the flower-like structured heterojunction prepared by Liwen Lei and colleagues could remove RhB (20 mg/L) in 20 min [34]. The as-prepared catalyst showed the best photoactivity among all the heterojunctions applied to RhB degradation. Compared to the former two studies, the major difference was its enlarged surface area. Therefore, it is reasonable to believe that larger surface area could enhance the degradation of pollutant under visible light illumination.

The similar results could be observed by other researchers. According to Qingbo Li, Wenwen Liu, and their colleagues [61,73], the as-prepared 010HB could remove MO in about three hours under visible light irradiation. Whereas, 001HB synthesized by Wenjie Shan and coworkers degraded MO in 5 h under similar conditions [75]. However, surface area might be the main factor that influences the degradation of MO under visible light illumination. The flower-like 001HB constructed by Xiaojing Wang and colleagues could degrade MO in 80 min [44], though it was 001 facet dominant. As all the experiments were conducted under similar conditions, it is reasonable to believe the enlarged surface area improved the photocatalytic performance of 001HB greatly.

Furthermore, the photodegradation rate of MB over pure g-C₃N₄ was higher than pure BiOCl, according to T. Jia and colleagues [65]. The removal efficiency of MB over as-prepared heterojunction was about two times higher than the pristine catalysts. The main reason might be that MB could not be photosensitized. The light absorption rate of the catalysts might play a more important role. S. Shi and colleagues also observed a

similar phenomenon, and the MB degradation rate over the as-prepared heterojunction of the two catalysts was about four times higher than the pristine materials [21].

Therefore, according to the articles discussed in this section, g-C₃N₄/BiOCl heterojunctions with 001 facet dominant BiOCl and enlarged surface area could appear superior in terms of dye degradation.

3.2. Other Applications

Besides dye degradation, other applications of the g-C₃N₄/BiOCl composite were seldom reported, as according to Table 5.

Table 5. Other applications of g-C₃N₄/BiOCl heterojunctions.

Catalyst (Mass Ratio %)	Application	Light Source	Efficiency/Time	Main Reactive Species	Stability and Reusability	Ref.
(OV)BiOCl/g-C ₃ N ₄ -10/BiOCl/g-C ₃ N ₄ (10/90)	Degradation of carbamazepine	Visible light	49%/240 min	•O ₂ ⁻ , hole	~50% after 5 irradiation cycles	[62]
	Degradation of nizatidine	LED (365 nm)	96%/30 min	•O ₂ ⁻ , hole	~92% after 5 irradiation cycles	[63]
(OV)BiOCl-g-C ₃ N ₄ (50/50)	Degradation of 4-chlorophenol	Short-arc xenon lamp 420 nm cutoff filter	95 %/2 h	•O ₂ ⁻ , hole	81% after 4 irradiation cycles	[71]
g-C ₃ N ₄ /BiOCl	degradation of dibutyl phthalate and methyl orange	500 W halogen tungsten lamp 420 nm cutoff filter	60%/300 min(DBP) 70%/300 min(MO)	-	stable after 4 irradiation cycles	[75]

One of the most important applications is the removal of recalcitrant industrial materials. 4-chlorophenol (4-CP) is an important material widely used in many areas. It could be used to manufacture sanitizers, germicides, precursors of pesticides, and dyes [82]. Just like other endocrine disruptors (bisphenol A (BPA), bisphenol S (BPS), and bisphenol F (BPF)), which are hazardous to the environment, they were employed by Q. Wang and co-workers to test the photocatalytic performance of the g-C₃N₄/BiOCl heterojunction [71]. It was indicated that the refractory pollutants could be mostly degraded within 2 h, while these endocrine disruptors were impossible to remove by conventional wastewater treatment.

As one of the plasticizers, about 60% of Dibutyl phthalate (DBP) was photodegraded over the g-C₃N₄/BiOCl catalyst within 300 min of visible light irradiation, according to W. Shan and colleagues [75]. Plasticizers, such as DBP, could adversely affect the neurodevelopment of infant and child, which is very hard to be degraded by normal wastewater treatment plants [83]. Photocatalysis is supposed to be an effective way to remove DBP from aqueous solution.

Degradation of the residual pharmaceutical agents is another application of the g-C₃N₄/BiOCl binary heterojunction. For example, carbamazepine, as a psychotropic and antiepileptic drug, is a recalcitrant and toxic chemical, which was adopted by researchers to test the photoactivity of the g-C₃N₄/BiOCl heterojunction [62]. It was indicated that the binary heterojunction showed more superior photoactivity than pure catalysts.

The contamination of antibiotics has drawn lots of attention in recent years. The amine-based pharmaceutical nizatidine, which could cause environmental problems, was applied in the field of photocatalysis by some researchers [63]. The result indicated that the degradation rate of the recalcitrant pollutant was accelerated over the g-C₃N₄/BiOCl photocatalyst. Application of antibiotic degradation, as one of the important applications of photocatalysis, is expected to have a bright future.

Moreover, according to B. Zhang and co-workers [84], g-C₃N₄/BiOCl could be used to modify an ITO electrode. That is the only application reported recently other than the degradation of recalcitrant pollutants.

However, it is not clear that if the same factors influenced the dye degradation could improve the removal of other chemicals, because there is still not enough research to be compared with.

According to Tables 4 and 5, the g-C₃N₄/BiOCl heterojunctions reviewed showed excellent stability and reusability. Almost every as-prepared catalyst exhibited stable photoactivity within at least five recycles. Furthermore, XRD patterns of the catalysts after several cycles showed that the crystal phase of the materials still stayed intact [21,58,61,71].

4. Mechanisms of the BiOCl/g-C₃N₄ Heterojunctions

P-type photocatalyst BiOCl combined with typical n-type photocatalyst g-C₃N₄ could form a conventional type-II photovoltaic with a staggered-gap band structure. There are three different types of semiconductor heterojunctions overall as shown in Figure 4. In a type-I heterojunction, conduction band (CB) and valence band (VB) of the semiconductor (SC1) are higher and lower than that of the other semiconductor (SC2), respectively. When SC1 and SC2 construct type-II heterojunction, CB and VB of SC1 are higher than of SC2. Because of the built-in electric field formed inside of the composite, photo-induced electrons tend to migrate to the CB of SC2. At the same time, holes accumulate on VB of SC1 rapidly. Because the electrons and holes migrate to different semiconductors, charge separation is enhanced. The pattern of charge carriers' movement in type-III heterojunction is the same as in type-II heterojunction. The difference of the band structures of the two semiconductors is even larger than in the type-II heterojunction [52].

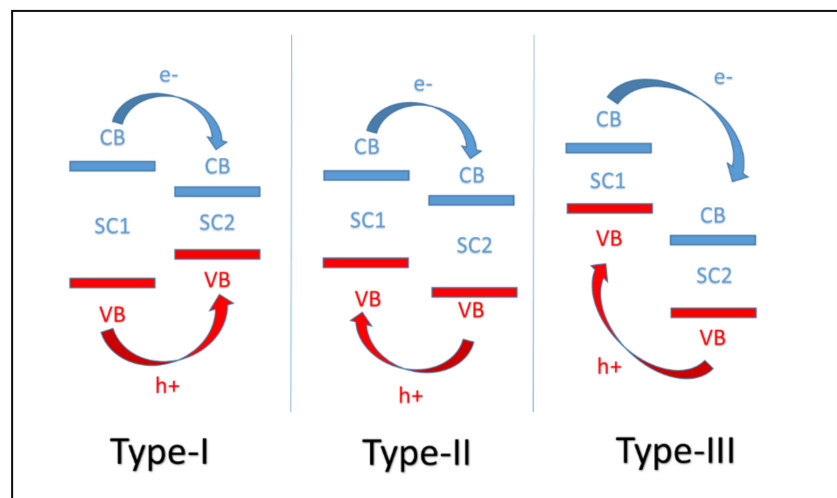


Figure 4. Three different types of semiconductor heterojunction.

Separation of electron-hole pairs could be prompted by the construction of the g-C₃N₄/BiOCl heterojunction. Solar energy utilization of the heterojunction was also more efficient since the wavelength of photo-response was broadened [8]. According to the articles reviewed, an interesting phenomenon is observed, some researchers believed that band structures of the two catalysts stayed unchanged after the combination of the two materials, whereas others thought that CB and VB of g-C₃N₄/BiOCl changed to align Fermi energy levels.

Theoretically, the Fermi energy level of an n-type catalyst is close to the bottom of CB. The Fermi energy level of a p-type catalyst is close to the top of VB [85]. After construction of heterojunction, the CB and VB of n-type catalyst tend to move downward, while those of p-type catalyst are moving upward. This kind of heterojunction based on g-C₃N₄ and BiOCl is labeled as PCNB in this article. The CB and VB of some g-C₃N₄/BiOCl heterojunctions stayed the same after the combination. This kind of heterojunction is denoted as the system of CNB here.

4.1. CNB Heterojunction

Generally, the proposed mechanism for the generation of reactive radicals on the surface of CNB heterojunction is shown in Figure 5. Photoexcited electrons firstly generated in the conduction band of $\text{g-C}_3\text{N}_4$ by irradiation of visible light because of its relatively mild band gap (2.7 eV). When it comes to dye degradation, photo-induced charge carriers also generated through dye sensitization. Then, electrons transferred to the conduction band of BiOCl because the conduction band of BiOCl is less negative than that of $\text{g-C}_3\text{N}_4$. Photogenerated electrons tend to transfer to a less negative conduction band. Electrons could react with O_2 on the surface of CNB to generate superoxide radicals. At the same time, holes remaining in the valence band of $\text{g-C}_3\text{N}_4$ react with surface-absorbed H_2O to generate hydroxyl radicals, so that separation of photo-generated charge carriers is improved and the catalyst can response to visible light. However, the redox ability of the heterojunction was sacrificed when photoactivity is improved, because the holes accumulated on VB of $\text{g-C}_3\text{N}_4$.

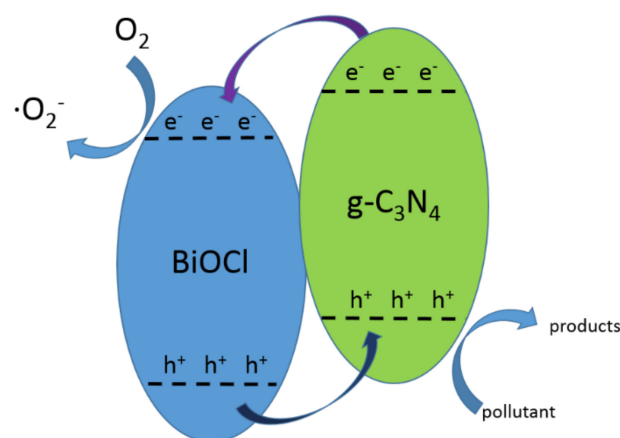


Figure 5. The mechanism for the generation of reactive radicals over CNB.

The mechanism mentioned above was adopted by Faisal Al Marzouqi and co-workers to explain the degradation of nizatidine over the BiOCl/ $\text{g-C}_3\text{N}_4$ heterojunction [63]. The degradation efficiency of nizatidine was improved under the irradiation of visible light. According to the XRD pattern, the as-prepared catalyst was constructed by pure BiOCl and $\text{g-C}_3\text{N}_4$. The construction of the heterojunction was verified. As shown in the UV-vis diffuse reflectance spectra, the absorption edge of BiOCl was about 364 nm (in the UV range), and that of $\text{g-C}_3\text{N}_4$ was about 450 nm (in the visible range). After being combined, the absorption band edge of the heterojunction could be up to 476 nm. The photoactivity of the heterojunction was improved. The bandgap value for 10% BiOCl/ $\text{g-C}_3\text{N}_4$ sample was 2.6 eV, which endowed the catalyst with the highest photoactivity among all the as-prepared samples. Therefore, the bandgap of the composite was narrowed by combination of the two components. The degradation rate of nizatidine was enhanced by the construction of the heterojunction as shown in Figure 6b. This improvement was explained by the double-charge transfer mechanism as proposed in Figure 5. Obviously, the CB and VB of both pristine catalysts did not change. The generation of reactive radicals depicted in the article was the same as that in Figure 5. However, the article provided no further evidence to prove the main reactive radicals. The presence of hydroxyl radicals was supposed to be the main cause of the degradation of nizatidine in the article. But the study did not exclude the possibility that the hydroxyl radicals could be generated from superoxide radicals. Y. Yang and colleagues demonstrated hydroxyl and superoxide radicals were the main species during the photocatalytic oxidation of MB, too [60]. Hydroxyl radicals were supposed to be produced in the VB of $\text{g-C}_3\text{N}_4$.

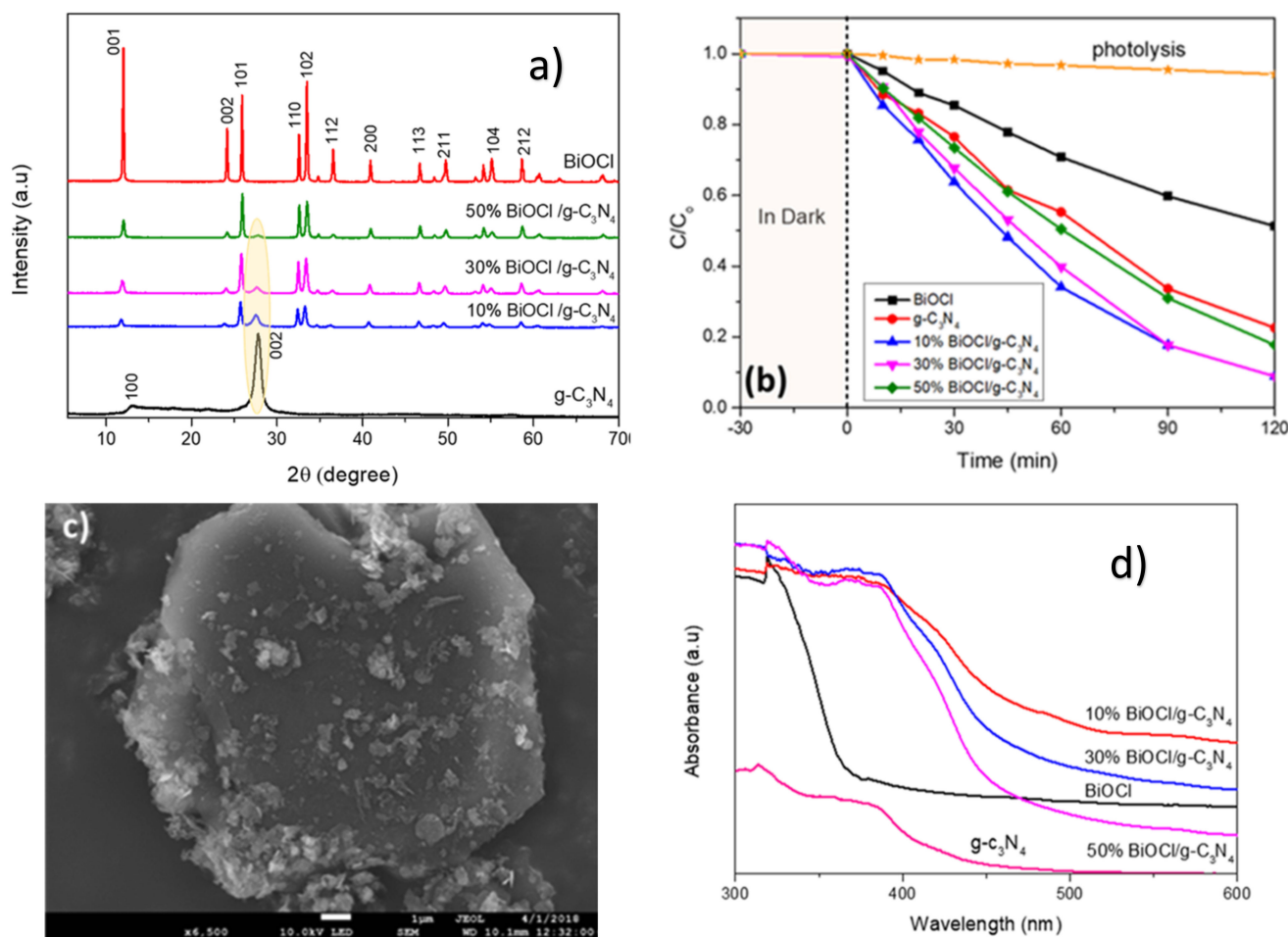


Figure 6. (a) XPR pattern of as-prepared BiOCl/g-C₃N₄ samples; (b) Degradation rate of nizatidine at an initial concentration of 5 mg/L and pH = 5.6 with all the prepared samples; (c) SEM image of 10% BiOCl/g-C₃N₄ sample; (d) UV-vis diffuse reflectance spectra of the obtained samples. Reproduced with permission from Al Marzouqi F et al, ACS Omega; published by American Chemical Society, 2013.

To date, lots of CNB heterojunctions were reported. Wenwen Liu and colleagues constructed a 2-dimensional layered BiOCl/g-C₃N₄ composite, and the photodegradation of MO was greatly improved through constructing a CNB heterojunction [73]. When the mass ratio of BiOCl reached 70%, BiOCl/g-C₃N₄ heterojunction showed the highest photocatalytic performance. EIS images and PL spectra were carried out to prove that better charge separation was realized. The proposed mechanism was similar to that shown in Figure 5. Electrons generated in the conduction band of g-C₃N₄, and then transferred to the conduction band of BiOCl. As a result, superoxide radicals generated on the surface of the heterojunction. Holes in the valence band of C₃N₄ were accumulated to participate in the degradation of MO degradation. Trapping experiments exhibited •O₂⁻ and holes were the main reactive species in the degradation of MO, which could be the evidence of the proposed mechanism. In this study, the VB and CB positions of BiOCl and g-C₃N₄ were determined by the Mott-Schottky curve. The alignment of band edges during the combination of the two materials was not taken into consideration, though the researchers did not directly adopt the standard values. The presence of the main reactive species was consistent with the proposed mechanism. Liwen Lei and co-workers prepared another heterostructure photocatalyst by combining BiOCl and g-C₃N₄ [34]. Arabic gum (AG) was added while synthesizing the heterojunction. They also proved that the superoxide and holes are the main reactive species through trapping experiments. The mechanism shown in Figure 5 was also adopted to explain the degradation of RhB over the composite.

However, the BiOCl/g-C₃N₄ heterojunction prepared by Xiaojing Wang and colleagues showed a different result [44]. Like the studies mentioned above [73], XPR, FT-IR spectroscopy, and PL emission spectra were carried out to demonstrate the formation of the heterojunction. The light response wavelength of BiOCl was broadened, while the charge separation was enhanced. Trapping experiments were also carried out to detect the main reactive species in the photocatalytic process. It turned out that •O₂⁻ was not the main reactive species, whereas holes played an important role during the degradation of MO.

Why the hydroxyl radicals were not generally supposed to generate during the photocatalytic reaction was not mentioned in the above studies. Zhang Sai and co-workers explained the reason in their study [86], the standard CB and VB potentials of g-C₃N₄ are approximately -1.3 and 1.40 eV, respectively. The standard redox potential of •O₂⁻/O₂ is -0.13 eV (vs. NHE), which is more positive than the CB potential of g-C₃N₄. So, it is very easy for e⁻ on the CB of g-C₃N₄ to generate superoxide radicals. The VB potential of g-C₃N₄ is less positive than the standard potential of •OH/OH⁻, which is +1.99 eV (vs. NHE). This makes holes on the VB of the catalyst and cannot be captured and to produce •OH radicals. If the CB and VB of the g-C₃N₄/BiOCl catalysts stay unchanged after the construction of the type-II heterojunction, electrons accumulate on the CB of BiOCl (-1.1 eV) [8] to form •O₂⁻. Holes migrate to the VB of g-C₃N₄, but cannot generate hydroxyl radicals. Therefore, superoxide radicals and holes are the main reactive species in the systems of BiOCl/g-C₃N₄. This theory is consistent with the results mentioned above. The work of L. Song and co-workers also suggested that the standard redox potential of the VB of g-C₃N₄ was not positive enough to generate •OH groups [69]. J. Sun and colleagues directly used the standard potentials of the pristine catalysts to describe the mechanism without taking the alignment of the Fermi energy level into account [68].

Q. Li and co-workers employed the result of X-ray photoelectron spectroscopy (VB XPS) spectra to determine the VB of pure g-C₃N₄, which was 1.44 eV NHE [61]. Compared to the standard potential of •OH/OH⁻, the generation of •OH was not expected to happen on the VB of g-C₃N₄. The result of trapping experiments suggested that •O₂⁻ and holes were the dominant reactive species during the degradation of MO.

Some other researchers did not only adopt trapping experiments to determine the main species, for example, L. Song and co-workers also adopted ESR spectra and trapping experiments to find out the main reactive species [59]. The presence of superoxide radicals was directly proved by the ESR test. The generation of hydroxyl radicals was not detected. Trapping experiments proved holes also played an important role during the oxidation of RhB.

Just like the aforementioned study of Xiaojing Wang and colleagues [44], T. Jia and colleagues determined the CB and VB potentials of BiOCl and g-C₃N₄ by using theoretical calculation, then holes were proved to be the main reactive species during the oxidation of MB through trapping experiments [65].

There are some other studies that adopted a similar mechanism to explain the degradation of pollutants over ternary catalysts based on the system of BiOCl/g-C₃N₄, like systems of BiOCl/g-C₃N₄/kaolinite [47], g-C₃N₄/CDs/BiOCl [48], BiOCl/CdS/g-C₃N₄ [87], and BiOI-BiOCl/C₃N₄ [88].

However, Xiaojuan Bai and colleagues demonstrated that hydroxyl radicals were still produced, though the VB of g-C₃N₄ was not positive enough [89]. They synthesized a kind of photocatalyst by modifying g-C₃N₄ with fullerene. After the modification, the degradation rate of MB was improved. Trapping and ESR experiments proved that holes and •OH were the main reactive species in the photodegradation of MB. After the modification, the VB of C₆₀/g-C₃N₄ was more positive by 0.17 eV. Considering the theory depicted above, that was not positive enough to generate •OH directly on the VB of g-C₃N₄. The mechanism was further researched by adding N₂ to create an anoxic suspension. The degradation of MB was almost unchanged in the presence of N₂, which indicated that the •OH was generated on the surface of the composite, but not through the reaction induced

by electrons on the CB of $\text{g-C}_3\text{N}_4$. This study seems contradictory to the theory described above that the VB of $\text{g-C}_3\text{N}_4$ was not positive enough to produce $\bullet\text{OH}$ [86].

The CNB system is a typical type-II heterojunction due to the band structures of the two materials. Trapping experiments were carried out to clarify the main reactive species, which proved to be superoxide radicals and holes. However, according to the study discussed above [86], there is still something unclear about the mechanism depicted in this section. Some more works are required to elucidate the reaction that happened over the heterojunction of CNB.

4.2. PCNB Heterojunction

According to the theory of semiconductor physics about p-n junction, n-type semiconductor $\text{g-C}_3\text{N}_4$ combines with p-type semiconductor BiOCl to form one composite, which tends to have one single Fermi energy level under one certain circumstance. As mentioned above, the Fermi level of $\text{g-C}_3\text{N}_4$ is supposed to be higher than that of BiOCl. After the construction of PCNB heterojunction, band structures of the two materials were expected to be changed to align the Fermi levels (EF). The photocatalytic mechanism of PCNB system is shown in Figure 7.

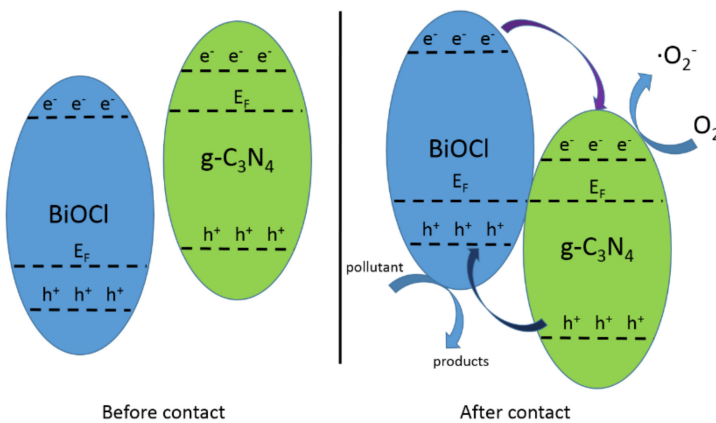


Figure 7. The schematic mechanism of $\text{g-C}_3\text{N}_4/\text{BiOCl}$ p-n junction.

Hybrid density-functional theory (DFT) calculation was used to anticipate the properties of the $\text{g-C}_3\text{N}_4/\text{BiOCl}$ composite [51]. $\text{g-C}_3\text{N}_4$ and BiOCl could form a stable composite with a narrower bandgap (2.1 eV), then the absorption of visible light was enhanced. According to the values of work function (WF), $\text{g-C}_3\text{N}_4$ and BiOCl were supposed to be positively and negatively charged after the contact, respectively, then the built-in electric field between the two materials was formed. Photo-induced charge carriers' separation was greatly improved since the lifetime of them was prolonged, and the recombination of electrons and holes was hindered in the system of $\text{g-C}_3\text{N}_4/\text{BiOCl}$. By the values of the valence and conduction band offset (VBO and CBO), which were 0.69 and 1.78 eV, respectively. The band structures of $\text{g-C}_3\text{N}_4$ and BiOCl were changed after contact as shown in Figure 7. Just as depicted above, theoretically, p-n junction possesses one single Fermi energy level, so energy bands of p-type semiconductor tend to move upward, whereas that of n-type semiconductor tend to move downward. Then, the as-prepared heterojunction can still be defined as a type-II heterojunction. Compared to pure catalysts, the photo response of PCNB heterojunction can be expanded to visible light region, and separation of photo-induced charge carriers could be promoted.

Though the author of the article mentioned above anticipated the properties of the binary heterojunction by theoretical calculation, many studies of other researchers could provide proof of the results. For example, Xianlong Zhang and co-workers synthesized a PCNB heterojunction by using $\text{g-C}_3\text{N}_4$ and BiOCl in the absence of the surfactant [72]. XRD data of the samples indicated that the formation of heterojunction did not change the

structure of pristine g-C₃N₄ and BiOCl as shown in Figure 8a. XPS analysis was carried out to prove the strong interaction between g-C₃N₄ and BiOCl in the heterojunction. UV-Vis DRS spectrum (Figure 8b) indicated the wavelength of light response was expanded to visible light region. The recombination of electrons and holes was inhibited by the construction of heterojunction, which could be inferred from the photoluminescence spectra shown in Figure 8d. The results of the trapping experiments indicated that the dominant reactive species in the degradation of RhB over the as-prepared catalysts was similar to that shown in Figure 7 which was different from that in Figure 5. The conduction band edge and valence band edge of BiOCl moved upward, while the band edges of g-C₃N₄ moved downward after the contact of the two materials. The experiments and tests conducted above verified the results of hybrid density-functional theory (DFT) calculation.

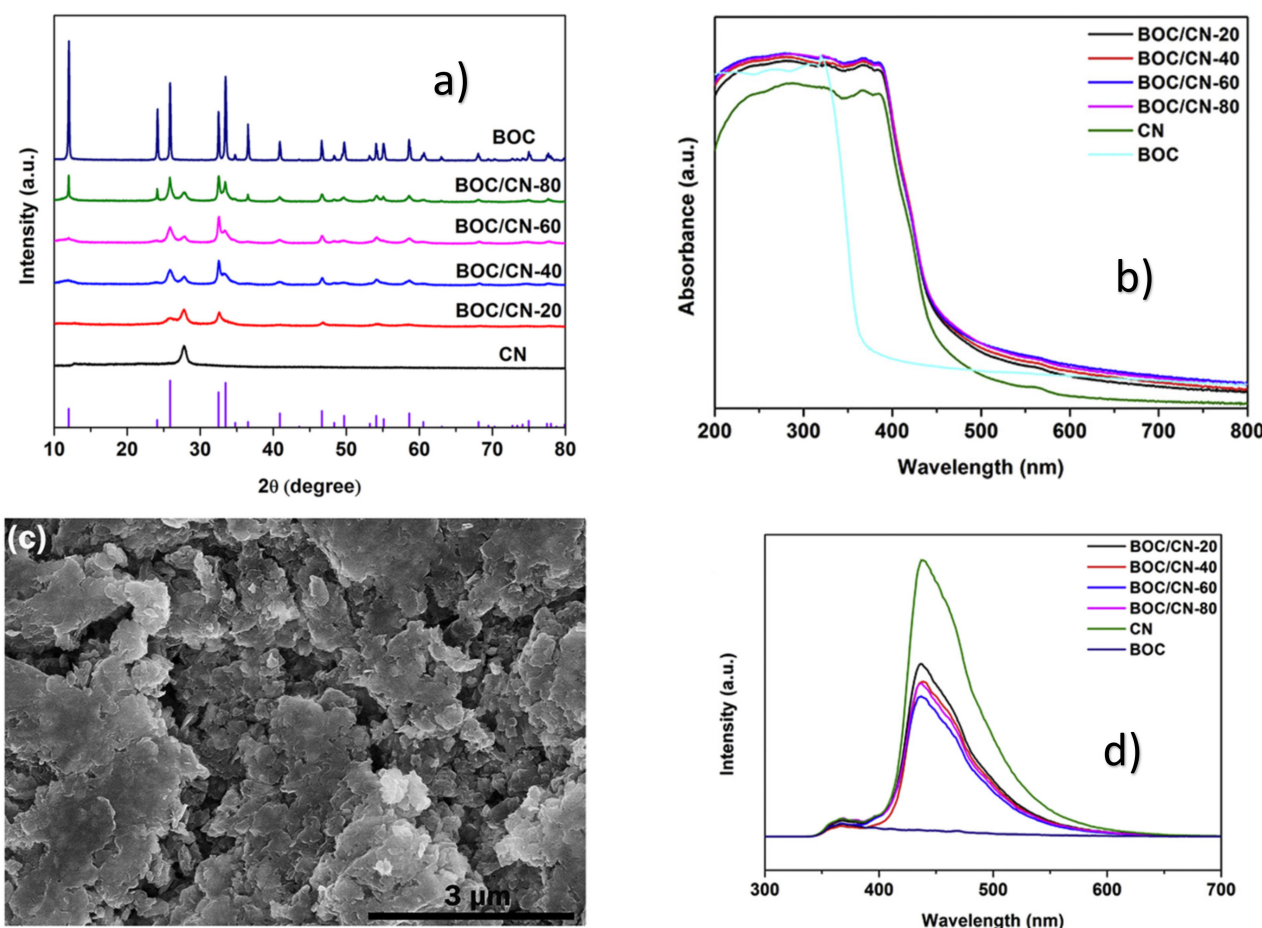


Figure 8. (a) XRD data, (b) UV-Vis DRS spectrum, (c) SEM, (d) photoluminescence spectra of all the samples. Reproduced with permission from Zhang X et al, Applied Surface Science; published by Elsevier BV, 2019.

Oxygen vacancies of PCNB were also introduced, which enhanced the photoactivity. Generally, oxygen vacancy is a common defect on oxide surfaces [90]. Oxygen vacancies could be introduced by certain methods. For example, removal of the surface oxygen atoms and elimination of the surface hydroxyl groups could be realized simultaneously through microwave irradiation and reaction between ethylene glycol and BiOCl [91]. However, there still is not a proper way to detect OVs quantitatively at present. The understanding of OVs is still infant. There are still many steps to take to elucidate the function of oxygen vacancy.

Qiao Wang and co-workers synthesized an oxygen vacancy-rich 2 D/2 D BiOCl/g-C₃N₄ p-n junction [71]. The efficiency of dechlorination and hydroxylation of 4-chlorophenol

over the as-prepared heterojunction were improved under the illumination of visible light. Notably, photoactivity of the catalyst was promoted greatly by introducing oxygen vacancies through the addition of the template of PVP. The presence of OVs could be detected by electron spin resonance (ESR) spectroscopy. Oxygen vacancy is a very common surface defect that exists on the surface of BiOCl, which could produce a new state in the bandgap and localize the photo-induced electrons [92]. The light absorption of BiOCl photocatalyst was expended to the visible light region in the presence of oxygen vacancies. Furthermore, OVs could facilitate the generation of superoxide radicals. Therefore, the introduction of OVs could improve the photoactivity of the catalyst. Other researchers used multiple methods to detect OVs. W. Hou and colleagues also synthesized another oxygen vacancy-rich PCNB heterojunction [62]. They not only employed ESR spectroscopy to prove the presence of OVs on the surface of the catalyst, but also adopted O₂-TPD profiles (Figure 9) to further detect the OVs. ESR and trapping experiments were also conducted to determine the main reactive species in the study, simultaneously.

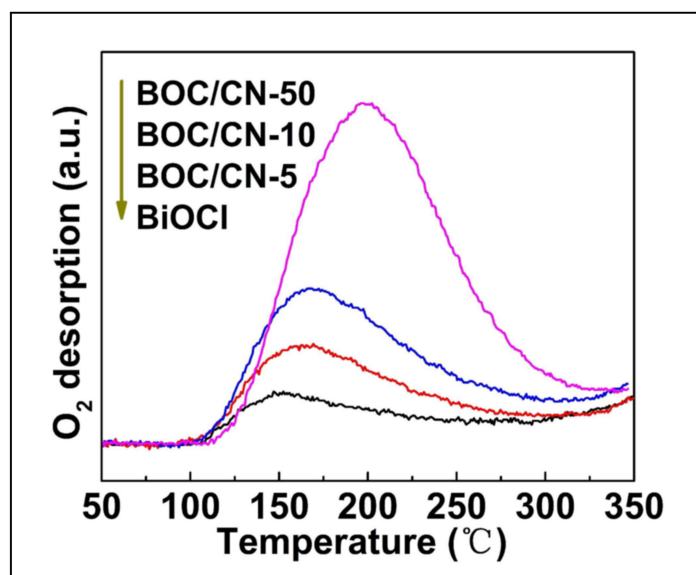


Figure 9. The O₂-TPD profiles of BiOCl, BOC/CN-5, BOC/CN-10, and BOC/CN-50. Reproduced with permission from Hou W et al, ChemistrySelect; published by John Wiley and Sons, 2020.

However, some researchers just adopted the mechanism depicted in Figure 7 to explain the photocatalytic reaction that happened over the g-C₃N₄/BiOCl heterojunction. For instance, Sheng Yin and co-workers synthesized a p-n junction g-C₃N₄/BiOCl with the assistance of ionic liquid [C16mim]Cl [74]. The characterization of as-prepared heterojunction showed the two materials constructed a stable heterojunction and stayed intact during the synthesis process. The photocatalytic performance of the composite was enhanced. However, the researchers did not use other methods, like trapping experiments, to prove the proposed mechanism.

In recent years, researchers have employed some advanced techniques to figure out the photocatalytic mechanism of the g-C₃N₄/BiOCl heterojunction. According to Z. Chen and co-workers, ultrafast transient absorption (TA) spectroscopy was adopted to test the mechanism [93]. TA spectroscopy provided more direct evidence of the PCNB heterojunction mechanism. Representative TA kinetic profiles indicated that the photo-induced electrons transferred to the CB of g-C₃N₄ in the binary heterojunction. If the band structures of the two photocatalysts stayed the same, the electrons were supposed to accumulate in the CB of BiOCl because of the more positive redox potential. It is reasonable to believe the results of TA spectroscopy could be the evidence of the PCNB mechanism.

Just like the study mentioned above [61], W. Cai and colleagues also adopted the valence band X-ray photoelectron spectroscopy (VB XPS) to determine the VB of BiOCl

and g-C₃N₄ [70]. However, the same technique was employed by both articles, which obtained different results. It was indicated that the alignment of the Fermi levels happened while preparing the g-C₃N₄/BiOCl composite. The photo-induced electrons gathered in the CB of g-C₃N₄, while the accumulation of the holes happened on the VB of BiOCl. The potential of the VB (1.58 eV) was not positive enough to produce •OH. It was reasonable to deduce that the superoxide radicals were the main reactive species.

4.3. Z-Scheme Heterojunction

Normally, whether the band structures of heterojunctions changed after contact with each other, these systems cannot have high-efficient charge separation and strong redox ability at the same time [94]. Many researchers tried to find a different way to produce a new form of photocatalyst, which possessed high-efficient charge separation without sacrificing the redox ability of pristine catalyst since the construction of heterojunction is a perfect way to improve the photoactivity. Z-scheme photocatalyst is such an ideal system. By combining two or more kinds of materials, the new composite could respond to visible light and the charge separation can be improved, but the redox abilities of these catalysts were unharmed, like the system of g-C₃N₄/Au/BiOCl [49] and BiOCl/RGO/protonated g-C₃N₄ [50]. Z-scheme photocatalysts could be synthesized by not only chemical methods but also mechanical force, just like the system of WO₃/NaNbO₃ [95]. According to Yang Bai and co-workers, directly combining g-C₃N₄ and BiOCl could construct a Z-scheme catalyst through a facile method [66]. Typically, Z-scheme catalysts can be divided into three types, which could be labeled as PS-C-PS, PS-PS, and PS-A/D-PS [96–98]. In the PS-A/D-PS system, there exists an acceptor/donor pair as a common electron mediator. The schematic diagram of Z-scheme electron transfer in the PS-A/D-PS system is shown in Figure 10(a).

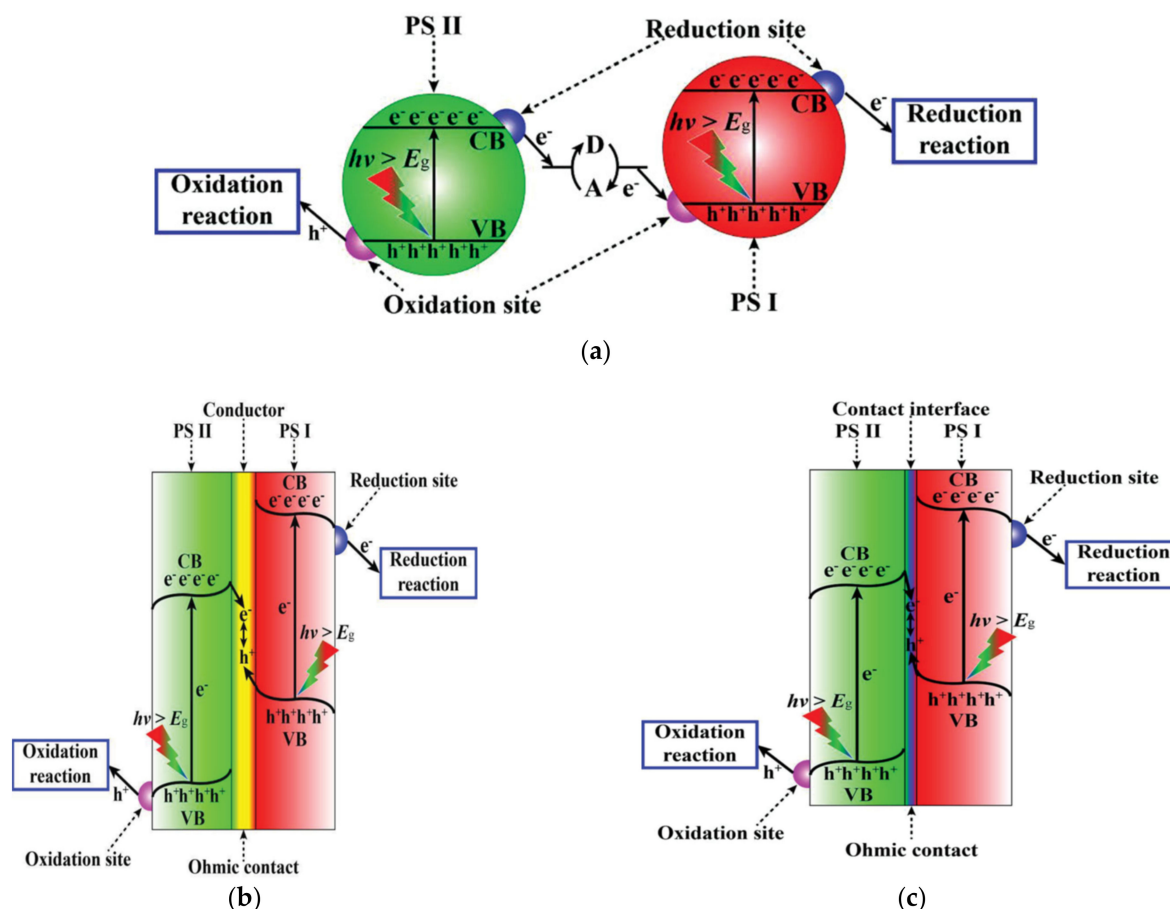


Figure 10. Schematic diagram of Z-scheme electron transfer in (a) PS-A/D-PS, (b) PS-C-PS, and (c) PS-PS system. Reproduced with permission from Zhou P et al, Advanced Materials; published by John Wiley and Sons, 2014.

Because the system of PS-C-PS is more stable than PS-A/D-PS, the PS-C-PS catalyst can be used in many different circumstances. Some researchers found the system of PS-A/D-PS was eroded after being used several times [99,100]. The PS-C-PS and PS-PS systems have a wider application range. These two systems also called all-solid-state Z-scheme photocatalysts. The schematic diagrams of Z-scheme electron transfer in the system of PS-C-PS and PS-PS are shown in Figure 10b,c.

The $\text{g-C}_3\text{N}_4/\text{Au}/\text{BiOCl}$ heterojunction could be classified as a typical PS-C-PS catalyst, Au was employed as the mediator. Z-scheme catalyst of $\text{g-C}_3\text{N}_4/\text{BiOCl}$ can be classified as a PS-PS type catalyst. It is believed that the conductive mediator of the PS-C-PS system could block the visible light to lower the efficiency of light energy absorption due to the surface plasmon resonance effect [101]. In this point of view, the system of PS-PS Z-scheme photocatalyst turns out to exhibit better photocatalysis performance. Because of the better photoactivity, Z-scheme catalysts drew a lot of attention, recently. Like the systems discussed in the former two sections, the enhancement of the Z-scheme catalysts based on $\text{g-C}_3\text{N}_4$ and BiOCl could be ascribed to better separation of charge carriers and wavelength expansion of light absorption.

To date, only one kind of Z-scheme $\text{g-C}_3\text{N}_4/\text{BiOCl}$ photocatalyst was reported [66]. The proposed catalytic mechanism of the $\text{BiOCl}/\text{g-C}_3\text{N}_4$ system is shown in Figure 11. The variation of the band structure during the synthesis of the heterojunction was not taken into account. Results of the trapping experiments indicated that the main reactive species were hydroxyl and superoxide radicals. This was considered as evidence of the formation of the Z-scheme heterojunction, according to the study.

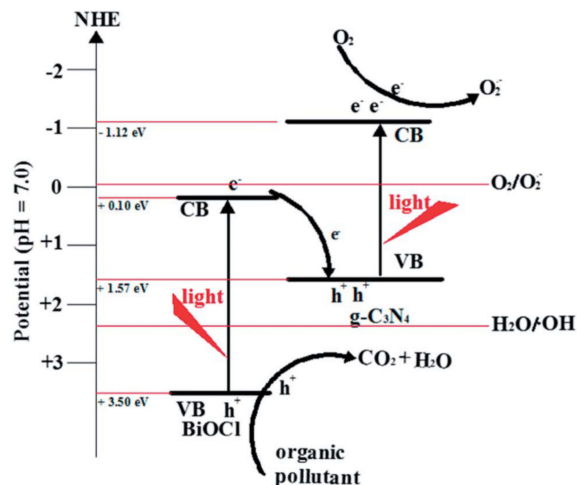


Figure 11. Direct Z-scheme photocatalytic mechanism of $\text{BiOCl}/\text{g-C}_3\text{N}_4$. Reproduced with permission from Bai Y et al, RSC Advances; published by Royal Society of Chemistry, 2014.

When the heterojunction was exposed under the illumination of visible light, the generation of $\bullet\text{OH}$ decreased. At the same time, the generation of superoxide radicals was not affected. The theoretical values of the band's redox potentials were directly adopted without being verified further.

The $\text{g-C}_3\text{N}_4/\text{Au}/\text{BiOCl}$ Z-scheme system also adopted a similar theory that considered that the band structures of the three materials stayed the same after combined. The main reactive species during the degradation of RhB was the photo-induced holes. The aforementioned study of $\text{BiOCl}/\text{RGO}/\text{protonated g-C}_3\text{N}_4$ also expected the band structures stayed the same during the formation of the heterojunction. The main reactive species of the antibiotic TC degradation were holes and $\bullet\text{O}_2^-$, and the presence of them was taken as the evidence of the Z-scheme mechanism.

Therefore, all the Z-scheme photocatalysts mentioned above did not take the alignment of Fermi energy levels during the synthesis of the heterojunctions into account. Then,

theoretical values of the redox potentials were adopted to explain the proposed mechanisms. The presence of specific reactive species was used as proof of the proposed mechanism.

It is common sense that the enhancement caused by the construction of the heterojunction is due to better charge separation and expended wavelength of light absorption. However, when it comes to the explanation of the mechanism, there are three different scenarios. As far as we know, the CB of BiOCl and the VB of g-C₃N₄ is not negative and positive enough to generate superoxide and hydroxyl radicals, respectively. However, just like the study mentioned above, though the VB of C₆₀/g-C₃N₄ was not supposed to be positive enough to produce hydroxyl radicals, the presence of hydroxyl radicals was still detected in an anoxic environment, which excluded the possibility that hydroxyl radicals might be produced from superoxide radicals. According to the CNB heterojunctions mentioned above, a similar phenomenon was observed. The ionic-liquid-assisted solvent-thermal route synthesized BiOCl/g-C₃N₄ generated hydroxyl radicals under the illumination of visible light [44], but the radicals might be produced in the VB of g-C₃N₄. The authors carried out no further tests to figure out the source of the radicals.

Additionally, some studies mentioned above might be explained by more than one mechanism. The improvement of the heterojunctions could be translated by all the three mechanisms. For example, the Z-scheme mechanism was used to describe photocatalytic reaction over the g-C₃N₄/BiOCl heterojunction [66], but it is still plausible to explain the process by the mechanism of CNB heterojunction. Photo-induced electrons and holes accumulated on the CB of BiOCl and the VB of g-C₃N₄, respectively. So, it is reasonable to think that the main species were superoxide radicals and holes according to the mechanism showed in Figure 5. The generation of •OH could be ascribed to •O₂⁻. The presence of 420 nm cutoff filter meant that BiOCl cannot be photo-excited, so the concentration of •O₂⁻ decreased, then the chain of the reaction generated •OH was cut off. The results of the experiments could be evidence of the relation between those two reactive species.

The photocatalytic reaction could be also explained by the mechanism of PCNB heterojunction. The band structures changed after being combined. The electrons and holes accumulated on the CB of g-C₃N₄ and the VB of BiOCl just as shown in Figure 6. The results of trapping experiments could be evidence of the PCNB mechanism. The generation of •OH could be ascribed to •O₂⁻, either.

Therefore, it is difficult to testify the charge transfer mechanism over the g-C₃N₄/BiOCl photocatalysts. However, there is still no direct evidence of the mechanisms mentioned above. All the theories used to explain them seem very reasonable. Although trapping experiments, ESR tests, and other methods could detect the presence of the main reactive species, we still cannot figure out exactly where they come from. So, there are still many steps to take in order to precisely describe the mechanism.

5. Other Methods to Improve Photoactivity of Catalysts Based on CN and BOC

There are many studies focused on how to further enhance the photoactivity of the g-C₃N₄/BiOCl system. For example, Chengyun Zhou and colleagues used carbon-doped g-C₃N₄ (CCN) to combine with BiOCl. Then, the as-prepared p-n heterojunction showed improved photoactivity through degradation of tetracycline (TC) [7]. Notably, the bandgap of BiOCl was modulated by adjusting the ratio of Cl and O to synthesize a catalyst with a mild bandgap (2.33 eV), which was denoted as Bi₁₂O₁₇Cl₂. The as-prepared Bi₁₂O₁₇Cl₂ was able to respond to visible light due to its narrowed band gap. Through integrating with carbon-doped g-C₃N₄, a heterojunction of CCN / Bi₁₂O₁₇Cl₂ was composed. CCN was integrated with Bi₁₂O₁₇Cl₂ to form a stable heterojunction, and each of the elements were uniformly distributed on the surface of the photocatalyst. The absorption of visible light and separation of photo-induced charge carriers was enhanced by the coupling of the two materials. The degradation of TC over the heterojunction was improved greatly compared to pure catalysts. The results of ESR proved the presence of •OH and •O₂⁻ during the degradation. Trapping experiments proved the presence of •OH, •O₂⁻, and holes affecting the degradation process. This study also

adopted the PCNB mechanism to explain the mineralization process. Those two materials formed a p-n junction after being integrated. The band structures were changed because of the construction of the composite. There are also many other ternary systems based on BiOCl/g-C₃N₄ that were synthesized, like BiOCl/Bi₂MoO₆/g-C₃N₄ [102], BiOCl/TiO₂-C₃N₄ [103], g-C₃N₄@BiOCl/Bi₁₂O₁₇Cl₂ [104], g-C₃N₄/oxygen-deficient BiOCl nanocomposite/graphene quantum dots [105], BiOCl/CdS/g-C₃N₄ [87], g-C₃N₄/BiOCl_xI_{1-x} [106], g-C₃N₄/BiOCl_xBr_{1-x} [107], BiOI/BiOCl/g-C₃N₄ [88], and Bi₂S₃/BiOCl/g-C₃N₄ [46]. Unlike the CCN/Bi₁₂O₁₇Cl₂ system, all the mechanisms of ternary systems mentioned above did not take the alignment of Fermi levels into account.

Ajay Kumara and co-workers also synthesized a new kind of heterostructure through constructing quaternary magnetic BiOCl/g-C₃N₄/Cu₂O/Fe₃O₄ nano-heterojunction [108]. According to the vibrating sample magnetometry (VSM) studies, the addition of Fe₃O₄ endowed the heterojunction to be separated from liquid magnetically. The bandgap of the heterojunction was 2.58 eV, which indicated that the as-prepared catalyst could respond to visible light. The recombination of the photo-induced charge carriers was greatly inhibited. The degradation rate over the quaternary heterojunction was about 2.7 and 2.4 times higher as BiOCl and g-C₃N₄, respectively. It was even 0.5 times higher than BiOCl/g-C₃N₄ binary heterojunction. The main reactive species in the photocatalytic process were •OH and •O₂⁻, according to the results of trapping experiments. The mechanism was as depicted in Figure 12. The alignment of the Fermi energy levels was considered to happen during the preparation. P-n junctions were considered to be formed at the g-C₃N₄/BiOCl interface and the g-C₃N₄/Cu₂O interface, respectively.

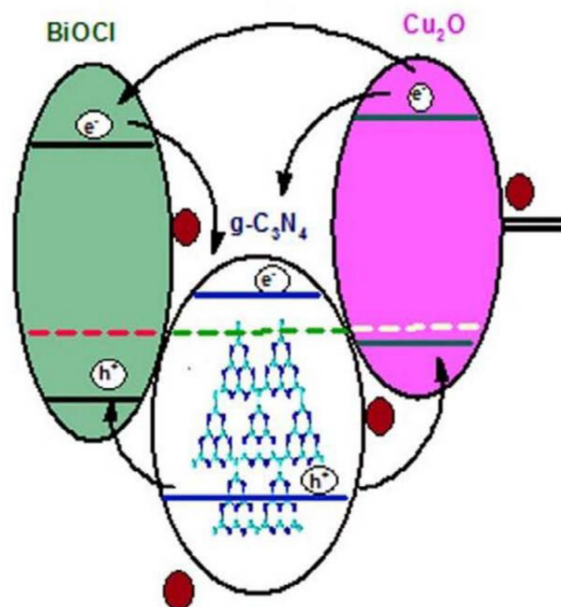


Figure 12. Proposed mechanism of quaternary heterojunction of BiOCl/g-C₃N₄/Cu₂O/Fe₃O₄. Reproduced with permission from Kumar A et al, Chemical Engineering Journal; published by Elsevier BV, 2018.

6. Summary and Outlook

According to the articles reviewed above, facet control and morphology of BiOCl were very important to the photoactivity of the heterojunctions. G-C₃N₄/BiOCl heterojunction with enlarged surface area accelerated the degradation of the azo dye. 010 facets exposed BiOCl of the heterojunction could enhance the absorption of the visible light.

BiOCl and g-C₃N₄ are both excellent photocatalysts despite their disadvantages, like fast photo-induced charge carriers' recombination and low efficient solar energy absorption. By coupling those two catalysts, we could get CNB heterojunction, PCNB heterojunction,

and Z-scheme heterojunction. A single catalyst cannot have all the advanced features simultaneously. The construction of catalysts based on g-C₃N₄/BiOCl is a good strategy to fabricate a perfect photocatalyst. Combining g-C₃N₄/BiOCl heterojunction with other materials could provide more active sites, and further improve its capability to respond to visible light or make the composite magnetic recyclable.

To date, the heterojunction based on BiOCl and g-C₃N₄ mainly used in the purification of water, according to the articles reviewed. The mechanisms used to explain the photocatalytic processes could be divided into three different scenarios. Though there were some researchers that employed certain advanced techniques to prove the source of the reactive species and the charge transfer over the as-prepared catalysts, there is still not enough direct evidence of the mechanisms. Gaining a clearer understanding of the charge transfer is very important for researchers to prepare better photocatalysts. The industrial application of photocatalysis will benefit from this direction of research. Nowadays, few researchers have focused on this direction. This article intends to inspire more studies to clarify the route of charge transfer.

Author Contributions: Conceptualization, investigation, resources, writing—original draft preparation, editing, Q.R.; writing—review, J.L.; supervision, Q.Y. and W.S. All authors have read and agreed to the published version of the manuscript.

Funding: This research received no external funding.

Conflicts of Interest: The authors declare no conflict of interest.

References

- Pan, M.; Wong, C.K.C.; Chu, L.M. Distribution of Antibiotics in Wastewater-Irrigated Soils and Their Accumulation in Vegetable Crops in the Pearl River Delta, Southern China. *J. Agric. Food Chem.* **2014**, *62*, 11062–11069. [[CrossRef](#)] [[PubMed](#)]
- Sharma, V.; Anquandah, G.A.K.; Yngard, R.A.; Kim, H.; Fekete, J.; Bouzek, K.; Ray, A.K.; Golovko, D. Nonylphenol, octylphenol, and bisphenol-A in the aquatic environment: A review on occurrence, fate, and treatment. *J. Environ. Sci. Health Part A* **2009**, *44*, 423–442. [[CrossRef](#)]
- Yesilada, O.; Asma, D.; Cing, S. Decolorization of textile dyes by fungal pellets. *Process. Biochem.* **2003**, *38*, 933–938. [[CrossRef](#)]
- Ahern, J.; Fairchild, R.; Thomas, J.S.; Carr, J.; Patterson, H.H. Characterization of BiOX compounds as photocatalysts for the degradation of pharmaceuticals in water. *Appl. Catal. B Environ.* **2015**, *179*, 229–238. [[CrossRef](#)]
- Sun, S.; Wang, W.; Zhang, L.; Zhou, L.; Yin, W.; Shang, M. Visible Light-Induced Efficient Contaminant Removal by Bi₅O₇I. *Environ. Sci. Technol.* **2009**, *43*, 2005–2010. [[CrossRef](#)]
- Chang, F.; Xie, Y.; Zhang, J.; Chen, J.; Li, C.; Wang, J.; Luo, J.; Deng, B.; Hu, X. Construction of exfoliated g-C₃N₄ nanosheets–BiOCl hybrids with enhanced photocatalytic performance. *RSC Adv.* **2014**, *4*, 28519–28528. [[CrossRef](#)]
- Zhou, C.; Lai, C.; Xu, P.; Zeng, G.; Huang, D.; Li, Z.; Zhang, C.; Cheng, M.; Hu, L.; Wan, J.; et al. Rational Design of Carbon-Doped Carbon Nitride/Bi₁₂O₁₇Cl₂ Composites: A Promising Candidate Photocatalyst for Boosting Visible-Light-Driven Photocatalytic Degradation of Tetracycline. *ACS Sustain. Chem. Eng.* **2018**, *6*, 6941–6949. [[CrossRef](#)]
- Yang, Y.; Zhang, C.; Lai, C.; Zeng, G.; Huang, D.; Cheng, M.; Wang, J.; Chen, F.; Zhou, C.; Xiong, W. BiOX (X = Cl, Br, I) photocatalytic nanomaterials: Applications for fuels and environmental management. *Adv. Colloid Interface Sci.* **2018**, *254*, 76–93. [[CrossRef](#)] [[PubMed](#)]
- Liu, Y.; Zhang, H.; Ke, J.; Zhang, J.; Tian, W.; Xu, X.; Duan, X.; Sun, P.H.; Tade, M.; Wang, S. 0D (MoS₂)/2D (g-C₃N₄) heterojunctions in Z-scheme for enhanced photocatalytic and electrochemical hydrogen evolution. *Appl. Catal. B Environ.* **2018**, *228*, 64–74. [[CrossRef](#)]
- Guo, F.; Shi, W.; Li, M.; Shi, Y.; Wen, H. 2D/2D Z-scheme heterojunction of CuInS₂/g-C₃N₄ for enhanced visible-light-driven photocatalytic activity towards the degradation of tetracycline. *Sep. Purif. Technol.* **2019**, *210*, 608–615. [[CrossRef](#)]
- Liang, S.; Zhang, D.; Pu, X.; Yao, X.; Han, R.; Yin, J.; Ren, X. A novel Ag₂O/g-C₃N₄ p-n heterojunction photocatalysts with enhanced visible and near-infrared light activity. *Sep. Purif. Technol.* **2019**, *210*, 786–797. [[CrossRef](#)]
- Liu, G.; Wang, G.; Hu, Z.; Su, Y.; Zhao, L. Ag₂O nanoparticles decorated TiO₂ nanofibers as a p-n heterojunction for enhanced photocatalytic decomposition of RhB under visible light irradiation. *Appl. Surf. Sci.* **2019**, *465*, 902–910. [[CrossRef](#)]
- Guo, F.; Shi, W.; Wang, H.; Han, M.; Guan, W.; Huang, H.; Liu, Y.; Kang, Z. Study on highly enhanced photocatalytic tetracycline degradation of type II AgI/CuBi₂O₄ and Z-scheme AgBr/CuBi₂O₄ heterojunction photocatalysts. *J. Hazard. Mater.* **2018**, *349*, 111–118. [[CrossRef](#)]
- Lai, C.; Zhang, M.; Li, B.; Huang, D.; Zeng, G.; Qin, L.; Liu, X.; Yi, H.; Cheng, M.; Li, L.; et al. Fabrication of CuS/BiVO₄ (0 4 0) binary heterojunction photocatalysts with enhanced photocatalytic activity for Ciprofloxacin degradation and mechanism insight. *Chem. Eng. J.* **2019**, *358*, 891–902. [[CrossRef](#)]

15. Zhu, C.; Zhang, L.; Jiang, B.; Zheng, J.; Hu, P.; Li, S.; Wu, M.; Wu, W. Fabrication of Z-scheme $\text{Ag}_3\text{PO}_4/\text{MoS}_2$ composites with enhanced photocatalytic activity and stability for organic pollutant degradation. *Appl. Surf. Sci.* **2016**, *377*, 99–108. [CrossRef]
16. Hao, Q.; Niu, X.; Nie, C.; Hao, S.; Zou, W.; Ge, J.; Chen, D.; Yao, W. A highly efficient $\text{g-C}_3\text{N}_4/\text{SiO}_2$ heterojunction: The role of SiO_2 in the enhancement of visible light photocatalytic activity. *Phys. Chem. Chem. Phys.* **2016**, *18*, 31410–31418. [CrossRef]
17. Nguyen, T.B.; Huang, C.; Doong, R.-A. Photocatalytic degradation of bisphenol A over a $\text{ZnFe}_2\text{O}_4/\text{TiO}_2$ nanocomposite under visible light. *Sci. Total Environ.* **2019**, *646*, 745–756. [CrossRef]
18. Luo, J.; Li, R.; Chen, Y.; Zhou, X.; Ning, X.; Zhan, L.; Ma, L.; Xu, X.; Xu, L.; Zhang, L. Rational design of Z-scheme $\text{LaFeO}_3/\text{SnS}_2$ hybrid with boosted visible light photocatalytic activity towards tetracycline degradation. *Sep. Purif. Technol.* **2019**, *210*, 417–430. [CrossRef]
19. He, R.; Zhou, J.; Fu, H.; Zhang, S.; Jiang, C. Room-temperature in situ fabrication of $\text{Bi}_2\text{O}_3/\text{g-C}_3\text{N}_4$ direct Z-scheme photocatalyst with enhanced photocatalytic activity. *Appl. Surf. Sci.* **2018**, *430*, 273–282. [CrossRef]
20. Chen, Y.; Zhu, G.; Hojamberdiev, M.; Gao, J.; Zhu, R.; Wang, C.; Wei, X.; Liu, P. Three-dimensional $\text{Ag}_2\text{O}/\text{Bi}_5\text{O}_7\text{I}$ p–n heterojunction photocatalyst harnessing UV–vis–NIR broad spectrum for photodegradation of organic pollutants. *J. Hazard. Mater.* **2018**, *344*, 42–54. [CrossRef]
21. Shi, S.; Gondal, M.; Al-Saadi, A.; Fajgar, R.; Kupcik, J.; Chang, X.; Shen, K.; Xu, Q.; Seddigi, Z. Facile preparation of $\text{g-C}_3\text{N}_4$ modified BiOCl hybrid photocatalyst and vital role of frontier orbital energy levels of model compounds in photoactivity enhancement. *J. Colloid Interface Sci.* **2014**, *416*, 212–219. [CrossRef] [PubMed]
22. Ong, W.-J.; Tan, L.-L.; Ng, Y.H.; Yong, S.-T.; Chai, S.-P. Graphitic Carbon Nitride ($\text{g-C}_3\text{N}_4$)-Based Photocatalysts for Artificial Photosynthesis and Environmental Remediation: Are We a Step Closer to Achieving Sustainability? *Chem. Rev.* **2016**, *116*, 7159–7329. [CrossRef]
23. Li, Y.; Zhang, C.; Shuai, D.; Naraginti, S.; Wang, D.; Zhang, W. Visible-light-driven photocatalytic inactivation of MS_2 by metal-free $\text{g-C}_3\text{N}_4$: Virucidal performance and mechanism. *Water Res.* **2016**, *106*, 249–258. [CrossRef]
24. Goettmann, F.; Fischer, A.; Antonietti, M.; Thomas, A. Metal-free catalysis of sustainable Friedel–Crafts reactions: Direct activation of benzene by carbon nitrides to avoid the use of metal chlorides and halogenated compounds. *Chem. Commun.* **2006**, 4530–4532. [CrossRef] [PubMed]
25. Wang, X.; Maeda, K.; Thomas, A.; Takanabe, K.; Xin, G.; Carlsson, J.M.; Domen, K.; Antonietti, M. A metal-free polymeric photocatalyst for hydrogen production from water under visible light. *Nat. Mater.* **2009**, *8*, 76–80. [CrossRef] [PubMed]
26. Liu, J.; Liu, Y.; Liu, N.; Han, Y.; Zhang, X.; Huang, H.; Lifshitz, Y.; Lee, S.-T.; Zhong, J.; Kang, Z. Metal-free efficient photocatalyst for stable visible water splitting via a two-electron pathway. *Science* **2015**, *347*, 970–974. [CrossRef]
27. Zheng, Y.; Liu, J.; Liang, J.; Jaroniec, M.; Qiao, S.Z. Graphitic carbon nitride materials: Controllable synthesis and applications in fuel cells and photocatalysis. *Energy Environ. Sci.* **2012**, *5*, 6717–6731. [CrossRef]
28. Pawar, R.; Kang, S.; Ahn, S.H.; Lee, C.S. Gold nanoparticle modified graphitic carbon nitride/multi-walled carbon nanotube ($\text{g-C}_3\text{N}_4/\text{CNTs}/\text{Au}$) hybrid photocatalysts for effective water splitting and degradation. *RSC Adv.* **2015**, *5*, 24281–24292. [CrossRef]
29. Lan, M.; Fan, G.; Yang, L.; Li, F. Enhanced visible-light-induced photocatalytic performance of a novel ternary semiconductor coupling system based on hybrid Zn-In mixed metal oxide/ $\text{g-C}_3\text{N}_4$ composites. *RSC Adv.* **2014**, *5*, 5725–5734. [CrossRef]
30. Huang, L.; Xu, H.; Li, Y.; Li, H.; Cheng, X.; Xia, J.; Xu, Y.; Cai, G. Visible-light-induced $\text{WO}_3/\text{g-C}_3\text{N}_4$ composites with enhanced photocatalytic activity. *Dalton Trans.* **2013**, *42*, 8606–8616. [CrossRef]
31. Wang, Y.; Wang, Z.; Muhammad, S.; He, J. Graphite-like C_3N_4 hybridized ZnWO_4 nanorods: Synthesis and its enhanced photocatalysis in visible light. *CrystEngComm* **2012**, *14*, 5065–5070. [CrossRef]
32. Xing, C.; Wu, Z.; Jiang, D.; Chen, M. Hydrothermal synthesis of $\text{In}_2\text{S}_3/\text{g-C}_3\text{N}_4$ heterojunctions with enhanced photocatalytic activity. *J. Colloid Interface Sci.* **2014**, *433*, 9–15. [CrossRef]
33. Han, G.; Li, D.Y.; Zheng, Y.F.; Song, X.C. Enhanced Visible-Light-Responsive Photocatalytic Properties of $\text{Bi}_2\text{MoO}_6\text{-BiOCl}$ Nanoplate Composites. *J. Nanosci. Nanotechnol.* **2018**, *18*, 5575–5581. [CrossRef]
34. Lei, L.; Gao, D.; Jin, H.; Zhang, Q.; Xu, J.; Fu, Z. A novel enhanced visible-light-driven photocatalyst via hybridization of nanosized BiOCl and graphitic C_3N_4 . *Dalton Trans.* **2015**, *44*, 795–803. [CrossRef] [PubMed]
35. Ramírez-Meneses, E.; Valencia-Barrón, J.P.; Hernández-Pérez, M.A.; Domínguez-Crespo, M.A.; Torres, A.; Palacios, E. Synthesis and Characterization of BiOCl Powders with Soft Templates. *J. Inorg. Organomet. Polym. Mater.* **2018**, *28*, 2350–2364. [CrossRef]
36. Lin, W.; Yu, X.; Shen, Y.; Chen, H.; Zhu, Y.; Zhang, Y.; Meng, H. Carbon dots/ BiOCl films with enhanced visible light photocatalytic performance. *J. Nanoparticle Res.* **2017**, *19*, 56. [CrossRef]
37. Singh, S.; Sharma, R.; Khanuja, M. A review and recent developments on strategies to improve the photocatalytic elimination of organic dye pollutants by BiOX ($X=\text{Cl}, \text{Br}, \text{I}, \text{F}$) nanostructures. *Korean J. Chem. Eng.* **2018**, *35*, 1955–1968. [CrossRef]
38. Yu, C.L.; Chen, J.C.; Zhou, W.Q.; Wei, L.F.; Fan, Q.Z. Grinding calcination preparation of WO_3/BiOCl heterostructures with enhanced visible light photocatalytic activity. *Mater. Res. Innov.* **2014**, *19*, 54–59. [CrossRef]
39. Cui, Z.; Song, H.; Ge, S.; He, W.; Liu, Y. Fabrication of $\text{BiOCl}/\text{BiOBr}$ hybrid nanosheets with enhanced superoxide radical dominating visible light driven photocatalytic activity. *Appl. Surf. Sci.* **2019**, *467*, 505–513. [CrossRef]
40. Junxiu, W.; Zhenzong, Z.; Xi, W.; Yi, S.; Yongfu, G.; Keung, W.P.; Renbi, B. Synthesis of novel p–n heterojunction m- $\text{Bi}_2\text{O}_4/\text{BiOCl}$ nanocomposite with excellent photocatalytic activity through ion-etching method. *Chin. J. Catal.* **2018**, *39*, 1792–1803.

41. Song, L.; Pang, Y.; Zheng, Y.; Chen, C.; Ge, L. Design, preparation and enhanced photocatalytic activity of porous BiOCl/BiVO₄ microspheres via a coprecipitation-hydrothermal method. *J. Alloys Compd.* **2017**, *710*, 375–382. [CrossRef]
42. Yu, L.; Zhang, X.; Li, G.; Cao, Y.; Shao, Y.; Li, D. Highly efficient Bi₂O₃CO₃/BiOCl photocatalyst based on heterojunction with enhanced dye-sensitization under visible light. *Appl. Catal. B Environ.* **2016**, *187*, 301–309. [CrossRef]
43. Zhong, Y.; Liu, Y.; Wu, S.; Zhu, Y.; Chen, H.; Yu, X.; Zhang, Y. Facile Fabrication of BiOI/BiOCl Immobilized Films with Improved Visible Light Photocatalytic Performance. *Front. Chem.* **2018**, *6*, 58. [CrossRef]
44. Wang, X.J.; Wang, Q.; Li, F.-T.; Yang, W.-Y.; Zhao, Y.; Hao, Y.-J.; Liu, S.-J. Novel BiOCl–C₃N₄ heterojunction photocatalysts: In situ preparation via an ionic-liquid-assisted solvent-thermal route and their visible-light photocatalytic activities. *Chem. Eng. J.* **2013**, *234*, 361–371. [CrossRef]
45. Zhang, C.; Li, Y.; Shuai, D.; Shen, Y.; Xiong, W.; Wang, L. Graphitic carbon nitride (g-C₃N₄)-based photocatalysts for water disinfection and microbial control: A review. *Chemosphere* **2019**, *214*, 462–479. [CrossRef] [PubMed]
46. Liu, S.; Liu, Y.; Dai, G.; Bao, X.; Huang, N.; Peng, R.; Zhou, Y. Synthesis and characterization of novel Bi₂S₃/BiOCl/g-C₃N₄ composite with efficient visible-light photocatalytic activity. *Mater. Lett.* **2019**, *241*, 190–193. [CrossRef]
47. Dong, X.; Sun, Z.; Zhang, X.; Li, C.; Zheng, S. Construction of BiOCl/g-C₃N₄/kaolinite composite and its enhanced photocatalysis performance under visible-light irradiation. *J. Taiwan Inst. Chem. Eng.* **2018**, *84*, 203–211. [CrossRef]
48. Asadzadeh-Khaneghah, S.; Habibi-Yangjeh, A.; Yubuta, K. Novel g-C₃N₄ nanosheets/CDs/BiOCl photocatalysts with exceptional activity under visible light. *J. Am. Ceram. Soc.* **2018**, *102*, 1435–1453. [CrossRef]
49. Zhao, S.; Zhang, Y.; Zhou, Y.; Fang, J.; Wang, Y.; Zhang, C.; Chen, W. Fabrication of sandwich-structured g-C₃N₄/Au/BiOCl Z-scheme photocatalyst with enhanced photocatalytic performance under visible light irradiation. *J. Mater. Sci.* **2018**, *53*, 6008–6020. [CrossRef]
50. Xue, J.; Li, X.; Ma, S.; Xu, P.; Wang, M.; Ye, Z. Facile fabrication of BiOCl/RGO/protonated g-C₃N₄ ternary nanocomposite as Z-scheme photocatalyst for tetracycline degradation and benzyl alcohol oxidation. *J. Mater. Sci.* **2018**, *54*, 1275–1290. [CrossRef]
51. Yao, W.; Zhang, J.; Wang, Y.; Ren, F. Hybrid density functional study on the mechanism for the enhanced photocatalytic properties of the ultrathin hybrid layered nanocomposite g-C₃N₄/BiOCl. *Appl. Surf. Sci.* **2018**, *435*, 1351–1360. [CrossRef]
52. Marschall, R. Semiconductor Composites: Strategies for Enhancing Charge Carrier Separation to Improve Photocatalytic Activity. *Adv. Funct. Mater.* **2014**, *24*, 2421–2440. [CrossRef]
53. Fu, J.; Yu, J.; Jiang, C.; Cheng, B. g-C₃N₄-Based Heterostructured Photocatalysts. *Adv. Energy Mater.* **2018**, *8*, 1701503. [CrossRef]
54. Xu, H.; Yan, J.; Xu, Y.; Song, Y.; Li, H.; Xia, J.; Huang, C.; Wan, H. Novel visible-light-driven AgX/graphite-like C₃N₄ (X=Br, I) hybrid materials with synergistic photocatalytic activity. *Appl. Catal. B Environ.* **2013**, *129*, 182–193. [CrossRef]
55. Iqbal, W.; Yang, B.; Zhao, X.; Rauf, M.; Waqas, M.; Gong, Y.; Zhang, J.; Mao, Y. Controllable synthesis of graphitic carbon nitride nanomaterials for solar energy conversion and environmental remediation: The road travelled and the way forward. *Catal. Sci. Technol.* **2018**, *8*, 4576–4599. [CrossRef]
56. Rono, N.; Kibet, J.K.; Martincigh, B.S.; Nyamori, V.O. A comparative study between thermal etching and liquid exfoliation of bulk graphitic carbon nitride to nanosheets for the photocatalytic degradation of a model environmental pollutant, Rhodamine B. *J. Mater. Sci. Mater. Electron.* **2021**, *32*, 687–706. [CrossRef]
57. Jiang, J.; Zhao, K.; Xiao, X.; Zhang, L. Synthesis and Facet-Dependent Photoreactivity of BiOCl Single-Crystalline Nanosheets. *J. Am. Chem. Soc.* **2012**, *134*, 4473–4476. [CrossRef] [PubMed]
58. Huang, Y. BiOCl Nanoplates Decorated on g-C₃N₄ for Enhanced Photocatalytic Activities. *Int. J. Electrochem. Sci.* **2017**, 4351–4359. [CrossRef]
59. Song, L.; Pang, Y.; Zheng, Y.; Ge, L. Hydrothermal synthesis of novel g-C₃N₄/BiOCl heterostructure nanodiscs for efficient visible light photodegradation of Rhodamine B. *Appl. Phys. A* **2017**, *123*, 500. [CrossRef]
60. Yang, Y.; Zhou, F.; Zhan, S.; Liu, Y.; Yin, Y. Enhanced Photocatalytic Activity of BiOCl Hybridized with g-C₃N₄. *J. Inorg. Organomet. Polym. Mater.* **2016**, *26*, 91–99. [CrossRef]
61. Li, Q.; Zhao, X.; Yang, J.; Jia, C.-J.; Jin, Z.; Fan, W. Exploring the effects of nanocrystal facet orientations in g-C₃N₄/BiOCl heterostructures on photocatalytic performance. *Nanoscale* **2015**, *7*, 18971–18983. [CrossRef]
62. Hou, W.; Deng, C.; Xu, H.; Li, D.; Zou, Z.; Xia, H.; Xia, D. n-p BiOCl@g-C₃N₄ Heterostructure with Rich-oxygen Vacancies for Photodegradation of Carbamazepine. *ChemistrySelect* **2020**, *5*, 2767–2777. [CrossRef]
63. AlMarzouqi, F.; Al Farsi, B.; Kuvarega, A.T.; Al Lawati, H.A.J.; Al Kindy, S.M.Z.; Kim, Y.; Selvaraj, R. Controlled Microwave-Assisted Synthesis of the 2D-BiOCl/2D-g-C₃N₄ Heterostructure for the Degradation of Amine-Based Pharmaceuticals under Solar Light Illumination. *ACS Omega* **2019**, *4*, 4671–4678. [CrossRef]
64. Tompsett, G.A.; Conner, W.C.; Yngvesson, K.S. Microwave Synthesis of Nanoporous Materials. *Chemphyschem Eur. J. Chem. Phys. Phys. Chem.* **2006**, *7*, 296–319. [CrossRef]
65. Jia, T.; Li, J.; Long, F.; Fu, F.; Zhao, J.; Deng, Z.; Wang, X.; Zhang, Y. Ultrathin g-C₃N₄ Nanosheet-Modified BiOCl Hierarchical Flower-Like Plate Heterostructure with Enhanced Photostability and Photocatalytic Performance. *Crystals* **2017**, *7*, 266. [CrossRef]
66. Bai, Y.; Wang, P.-Q.; Liu, J.-Y.; Liu, X.-J. Enhanced photocatalytic performance of direct Z-scheme BiOCl–g-C₃N₄ photocatalysts. *RSC Adv.* **2014**, *4*, 19456–19461. [CrossRef]
67. Zheng, C.-Z.; Zhang, C.-Y.; Zhang, G.-H.; Zhao, D.-J.; Wang, Y.-Z. Enhanced photocatalytic performance of g-C₃N₄ with BiOCl quantum dots modification. *Mater. Res. Bull.* **2014**, *55*, 212–215. [CrossRef]

68. Sun, J.; Song, J.; Gondal, M.A.; Shi, S.; Lu, Z.; Xu, Q.; Chang, X.; Xiang, D.; Shen, K. Preparation of g-C₃N₄/BiOX (X = Cl, Br, I) composites, and their photocatalytic activity under visible light irradiation. *Res. Chem. Intermed.* **2014**, *41*, 6941–6955. [CrossRef]
69. Song, L.; Zheng, Y.; Chen, C. Sonication-assisted deposition–precipitation synthesis of graphitic C₃N₄/BiOCl heterostructured photocatalysts with enhanced rhodamine B photodegradation activity. *J. Mater. Sci. Mater. Electron.* **2017**, *28*, 15861–15869. [CrossRef]
70. Cai, W.; Tang, J.; Shi, Y.; Wang, H.; Jiang, X. Improved in Situ Synthesis of Heterostructured 2D/2D BiOCl/g-C₃N₄ with Enhanced Dye Photodegradation under Visible-Light Illumination. *ACS Omega* **2019**, *4*, 22187–22196. [CrossRef] [PubMed]
71. Wang, Q.; Wang, W.; Zhong, L.; Liu, D.; Cao, X.; Cui, F. Oxygen vacancy-rich 2D/2D BiOCl-g-C₃N₄ ultrathin heterostructure nanosheets for enhanced visible-light-driven photocatalytic activity in environmental remediation. *Appl. Catal. B Environ.* **2018**, *220*, 290–302. [CrossRef]
72. Zhang, X.; An, D.; Feng, D.; Liang, F.; Chen, Z.; Liu, W.; Yang, Z.; Xian, M. In situ surfactant-free synthesis of ultrathin BiOCl/g-C₃N₄ nanosheets for enhanced visible-light photodegradation of rhodamine B. *Appl. Surf. Sci.* **2019**, *476*, 706–715. [CrossRef]
73. Liu, W.; Qiao, L.; Zhu, A.; Liu, Y.; Pan, J. Constructing 2D BiOCl/C₃N₄ layered composite with large contact surface for visible-light-driven photocatalytic degradation. *Appl. Surf. Sci.* **2017**, *426*, 897–905. [CrossRef]
74. Yin, S.; Di, J.; Li, M.; Sun, Y.; Xia, J.; Xu, H.; Fan, W.; Li, H. Ionic liquid-assisted synthesis and improved photocatalytic activity of p-n junction g-C₃N₄/BiOCl. *J. Mater. Sci.* **2016**, *51*, 4769–4777. [CrossRef]
75. Shan, W.; Hu, Y.; Bai, Z.; Zheng, M.; Wei, C. In situ preparation of g-C₃N₄/bismuth-based oxide nanocomposites with enhanced photocatalytic activity. *Appl. Catal. B Environ.* **2016**, *188*, 1–12. [CrossRef]
76. Wang, L.; Liu, X.; Luo, J.; Duan, X.; Crittenden, J.; Liu, C.; Zhang, S.; Pei, Y.; Zeng, Y.; Duan, X. Self-Optimization of the Active Site of Molybdenum Disulfide by an Irreversible Phase Transition during Photocatalytic Hydrogen Evolution. *Angew. Chem. Int. Ed. Engl.* **2017**, *56*, 7610–7614. [CrossRef]
77. Che, H.; Che, G.; Dong, H.; Hu, W.; Hu, H.; Liu, C.; Li, C. Fabrication of Z-scheme Bi₃O₄Cl/g-C₃N₄ 2 D/2 D heterojunctions with enhanced interfacial charge separation and photocatalytic degradation various organic pollutants activity. *Appl. Surf. Sci.* **2018**, *455*, 705–716. [CrossRef]
78. Adepu, A.K.; Anumula, R.; Narayanan, V. Photocatalytic degradation of Rhodamine B over a novel mesoporous titanosilicate/g-C₃N₄ nanocomposite under direct sunlight irradiation. *Microporous Mesoporous Mater.* **2017**, *247*, 86–94. [CrossRef]
79. Cheng, H.; Huang, B.; Dai, Y. Engineering BiOX (X = Cl, Br, I) nanostructures for highly efficient photocatalytic applications. *Nanoscale* **2014**, *6*, 2009–2026. [CrossRef]
80. Collivignarelli, M.C.; Abbà, A.; Miino, M.C.; Damiani, S. Treatments for color removal from wastewater: State of the art. *J. Environ. Manag.* **2019**, *236*, 727–745. [CrossRef] [PubMed]
81. Chiu, Y.-H.; Chang, T.-F.M.; Chen, C.-Y.; Sone, M.; Hsu, Y.-J. Mechanistic Insights into Photodegradation of Organic Dyes Using Heterostructure Photocatalysts. *Catalysts* **2019**, *9*, 430. [CrossRef]
82. Descomme, C. Catalytic wastewater treatment: Oxidation and reduction processes. Recent studies on chlorophenols. *Catal. Today* **2017**, *297*, 324–334. [CrossRef]
83. Radke, E.; Braun, J.M.; Nachman, R.M.; Cooper, G.S. Phthalate exposure and neurodevelopment: A systematic review and meta-analysis of human epidemiological evidence. *Environ. Int.* **2020**, *137*, 105408. [CrossRef] [PubMed]
84. Zhang, B.; Jia, Y.; Wang, J.; Hu, X.; Zhao, Z.; Cheng, Y. Cysteine-assisted photoelectrochemical immunoassay for the carcinoembryonic antigen by using an ITO electrode modified with C₃N₄-BiOCl semiconductor and CuO nanoparticles as antibody labels. *Microchim. Acta* **2019**, *186*, 633. [CrossRef] [PubMed]
85. Wang, H.; Zhang, L.; Chen, Z.; Hu, J.; Li, S.; Wang, Z.; Liu, J.; Wang, X. Semiconductor heterojunction photocatalysts: Design, construction, and photocatalytic performances. *Chem. Soc. Rev.* **2014**, *43*, 5234–5244. [CrossRef]
86. Zhang, S.; Gu, P.; Ma, R.; Luo, C.; Wen, T.; Zhao, G.; Cheng, W.; Wang, X. Recent developments in fabrication and structure regulation of visible-light-driven g-C₃N₄-based photocatalysts towards water purification: A critical review. *Catal. Today* **2019**, *335*, 65–77. [CrossRef]
87. Bellamkonda, S.; Rao, G.R. Nanojunction-mediated visible light photocatalytic enhancement in heterostructured ternary BiOCl/CdS/g-C₃N₄ nanocomposites. *Catal. Today* **2019**, *321–322*, 18–25. [CrossRef]
88. Aghdam, S.M.; Haghghi, M.; Allahyari, S.; Yosefi, L. Precipitation dispersion of various ratios of BiOI/BiOCl nanocomposite over g-C₃N₄ for promoted visible light nanophotocatalyst used in removal of acid orange 7 from water. *J. Photochem. Photobiol. A Chem.* **2017**, *338*, 201–212. [CrossRef]
89. Bai, X.; Wang, L.; Wang, Y.; Yao, W.; Zhu, Y. Enhanced oxidation ability of g-C₃N₄ photocatalyst via C60 modification. *Appl. Catal. B Environ.* **2014**, *152–153*, 262–270. [CrossRef]
90. Li, H.; Li, J.; Ai, Z.; Jia, F.; Zhang, L. Oxygen Vacancy-Mediated Photocatalysis of BiOCl: Reactivity, Selectivity, and Perspectives. *Angew. Chem. Int. Ed.* **2018**, *57*, 122–138. [CrossRef]
91. Li, H.; Zhang, L. Oxygen vacancy induced selective silver deposition on the {001} facets of BiOCl single-crystalline nanosheets for enhanced Cr(vi) and sodium pentachlorophenate removal under visible light. *Nanoscale* **2014**, *6*, 7805–7810. [CrossRef]
92. Li, H.; Shang, J.; Zhu, H.; Yang, Z.; Ai, Z.; Zhang, L. Oxygen Vacancy Structure Associated Photocatalytic Water Oxidation of BiOCl. *ACS Catal.* **2016**, *6*, 8276–8285. [CrossRef]

93. Chen, Z.; Zhang, Q.; Luo, Y. Determining the Charge-Transfer Direction in a p-n Heterojunction BiOCl/g-C₃N₄ Photocatalyst by Ultrafast Spectroscopy. *ChemPhotoChem* **2017**, *1*, 350–354. [[CrossRef](#)]
94. Natarajan, T.S.; Thampi, K.R.; Tayade, R.J. Visible light driven redox-mediator-free dual semiconductor photocatalytic systems for pollutant degradation and the ambiguity in applying Z-scheme concept. *Appl. Catal. B Environ.* **2018**, *227*, 296–311. [[CrossRef](#)]
95. Guo, Q.; Li, H.; Zhang, Q.; Zhang, Y. Fabrication, characterization and mechanism of a novel Z-scheme Ag₃PO₄/NG/polyimide composite photocatalyst for microcystin-LR degradation. *Appl. Catal. B Environ.* **2018**, *229*, 192–203. [[CrossRef](#)]
96. Maeda, K. Z-Scheme Water Splitting Using Two Different Semiconductor Photocatalysts. *ACS Catal.* **2013**, *3*, 1486–1503. [[CrossRef](#)]
97. Abe, R.; Sayama, K.; Sugihara, H. Development of New Photocatalytic Water Splitting into H₂ and O₂ Using Two Different Semiconductor Photocatalysts and a Shuttle Redox Mediator IO₃[−]/I[−]. *J. Phys. Chem. B* **2005**, *36*, 16052–16061. [[CrossRef](#)]
98. Zhou, P.; Yu, J.; Jaroniec, M. All-Solid-State Z-Scheme Photocatalytic Systems. *Adv. Mater.* **2014**, *26*, 4920–4935. [[CrossRef](#)]
99. Sayama, K.; Mukasa, K.; Abe, R.; Abe, Y.; Arakawa, H. A new photocatalytic water splitting system under visible light irradiation mimicking a Z-scheme mechanism in photosynthesis. *J. Photochem. Photobiol. A Chem.* **2002**, *148*, 71–77. [[CrossRef](#)]
100. Sayama, K.; Mukasa, K.; Abe, R.; Abe, Y.; Arakawa, H. Stoichiometric water splitting into H₂ and O₂ using a mixture of two different photocatalysts and an IO₃[−]/I[−] shuttle redox mediator under visible light irradiation. *Chem. Commun.* **2001**, 2416–2417. [[CrossRef](#)]
101. Tada, H.; Mitsui, T.; Kiyonaga, T.; Akita, T.; Tanaka, K. All-solid-state Z-scheme in CdS–Au–TiO₂ three-component nanojunction system. *Nat. Mater.* **2006**, *5*, 782–786. [[CrossRef](#)] [[PubMed](#)]
102. Zhao, W.; Wang, A.; Wang, Y.; Lv, C.; Zhu, W.; Dou, S.; Wang, Q.; Zhong, Q. Accessible fabrication and mechanism insight of heterostructured BiOCl/Bi₂MoO₆/g-C₃N₄ nanocomposites with efficient photosensitized activity. *J. Alloys Compd.* **2017**, *726*, 164–172. [[CrossRef](#)]
103. Shakeel, M.; Zhang, X.; Yasin, G.; Arif, M.; Abbas, Z.; Zaman, U.; Li, B. Fabrication of Amorphous BiOCl/TiO₂-C₃N₄ Heterostructure for Efficient Water Oxidation. *ChemistrySelect* **2019**, *4*, 8277–8282. [[CrossRef](#)]
104. Zhang, W.; Liang, Y. Facile Synthesis of Ternary g-C₃N₄@BiOCl/Bi₁₂O₁₇Cl₂ Composites with Excellent Visible Light Photocatalytic Activity for NO Removal. *Front. Chem.* **2019**, *7*, 231. [[CrossRef](#)] [[PubMed](#)]
105. Choi, J.U.; Jo, W.-K. g-C₃N₄/oxygen-deficient BiOCl nanocomposite assisted by distinguished properties of graphene quantum dots for the efficient photocatalytic removal of organic vapors. *Appl. Surf. Sci.* **2019**, *493*, 873–881. [[CrossRef](#)]
106. Hu, X.; Zhang, Y.; Wang, B.; Li, H.; Dong, W. Novel g-C₃N₄/BiOCl_xI_{1-x} nanosheets with rich oxygen vacancies for enhanced photocatalytic degradation of organic contaminants under visible and simulated solar light. *Appl. Catal. B Environ.* **2019**, *256*, 117789. [[CrossRef](#)]
107. Feng, Y.; Du, Y.; Du, M.; Tian, X.; Jiang, N.; Liu, Y. Synthesis and enhanced visible light photocatalytic activity of g-C₃N₄/BiOCl_xBr_{1-x} heterojunctions with adjustable energy band structure. *J. Phys. Chem. Solids* **2019**, *132*, 222–229. [[CrossRef](#)]
108. Kumar, A.; Kumar, A.; Sharma, G.; Al-Muhtaseb, A.H.; Naushad, M.; Ghfar, A.A.; Stadler, F.J. Quaternary magnetic BiOCl/g-C₃N₄/Cu₂O/Fe₃O₄ nano-junction for visible light and solar powered degradation of sulfamethoxazole from aqueous environment. *Chem. Eng. J.* **2018**, *334*, 462–478. [[CrossRef](#)]